Athermal and Thermal Lattice Gas Cellular Automata

by

Oleh Baran
Department of Physics, McGill University
Montréal, Québec
July 1995

A Thesis submitted to the
Faculty of Graduate Studies and Research
in partial fulfillment of the requirements for the degree of
Master of Science

Abstract

The Lattice Gas Cellular Automata method is a useful approximation for modeling fluids. It deals with systems of particles that move with a discrete set of velocities from site to site on a regular lattice. Such systems show fluid-like behavior in the appropriate limit.

We first study the theory of LGCA using the conventional methods of Statistical Mechanics. We start from the microcanonical description of LGCA and investigate the conditions for fluid-like macroscopic behavior. We consider the most important quantities for the description of fluids, namely the kinetic propagator, and the dynamic structure factor which is the power spectrum of density fluctuations. We give the Green-Kubo approximation for the transport coefficients of LGCA models and investigate the effects of velocity and space discretization on the theory of transport phenomena.

Next we compare the theoretical predictions with empirical results obtained from the numerical study of the Boltzmann collision matrix and from numerical simulations of the simple athermal FHP-1 model. We find agreement between the theoretical predictions of the transport properties and the results of such numerical investigations.

We also studied the more complicated thermal 19-bit model, introduced by Grosfils *et.al.* We show the importance of selecting appropriate collision processes to obtain fluid-like macroscopic behavior of the model.

Finally, we discuss the advantages and disadvantages of the various models in the light of our results.

Résumé

La méthode des automates cellulaires sur réseau (ACR) est une approximation très utile à la modélisation des fluides. Les ACR sont des systèmes de particules qui se déplacent avec une gamme de vitesses discrètes d'un site à l'autre sur un réseau régulier. De tels systèmes présentent un comportement de fluide dans la limite appropriée.

La théorie des ACR est d'abord étudiée en utilisant les méthodes habituelles de la mécanique statistique. Nous commençons par une description microcanonique des ACR et nous examinons les conditions nécessaires pour reproduire le comportement d'un fluide. Nous considérons les quantités les plus importantes pour la description des fluides, à savoir le propagateur cinétique et le facteur de structure dynamique qui est le spectre de puissance des fluctuations de densité. Nous donnons l'approximation de Green-Kubo pour les coefficients de transport des modèles d'ACR et examinons les effets de la discrétisation de l'espace et des vitesses sur la théorie des phénomènes de transport.

Les prédictions théoriques sont ensuite comparées avec les résultats empiriques obtenus de l'étude numérique de la matrice de collision de Boltzmann et de simulations numériques du modèle simple athermique FHP-1. Nous trouvons un accord entre les prédictions théoriques des propriétés de transport et les résultats de telles recherches numériques.

Le modèle thermique plus compliqué, dit des 19 bits, introduit par Grosfils *et al.* est aussi étudié. Nous montrons l'importance de choisir les processus de collision appropriés afin d'obtenir un modèle dont le comportement macroscopique est celui d'un fluide.

Finalement, nous discutons des avantages et des inconvénients des divers modèles à la lumière de nos résultats.

Acknowledgments

This work could not have been completed without the help of many people, some of whom I would now like to thank.

I would like to take this opportunity to thank my thesis supervisor, Professor Richard Harris, for introducing me to this project, for supporting me throughout the course of the research, for the patience he has shown during the research, and for a great deal of editorial help in the writing of this thesis. I have benefited greatly from his advice and encouragement.

At McGill I received help from almost all the members of the Condensed Matter Physics group. Thanks are due to Martin-D. Lacasse for help in managing the gnuplot drawing package used in the creation of many plots in this thesis, for help in solving many LaTeX problems and for many other valuable computer tips ; to Eric Dufresne who helped with xwplot software which I used to produce most of the two-dimensional plots presented in this thesis; to Karim Aguenaou who translated the abstract; to Rita Koknaeva who kindly offered her PC computer during "system shut-downs"; to Juan Gallego who provided computer help and at one occasion recovered all my valuable directories with data files which I accidently deleted; to Mikko Karttune who introduced me to the WWW network where I found a lot of valuable information related (and not related) to my thesis.

Thanks also to all the people in the Room 421, who contributed in many possible direct and indirect ways to this thesis, to McGill physics soccer and volleyball team members for providing good recreation.

For assistance in dealing with all the administrative work, I thank Paula Domingues, Diane Koziol and Joanne Longo.

I also thank the Faculty of Graduate Studies at McGill University for financial support through Tuition Fee Waivers.

Finally, I would like to thank my parents in Ukraine, who have given me enormous support and encouragement even from far away, and to my aunt Marta in Toronto for all her support during my stay at McGill.

Contents

List of Figures

Chapter 1

Review of Lattice Gas Theory

1.1 General approach to Lattice Gas Theory

Numerical methods for fluid dynamics now occupy an important place in the science of fluids. A major stimulus to the field has been the large number of applications in which fluid flows play a crucial role, and this has spurred the interest of numerous physicists, computational engineers and mathematicians.

In particular, methods that solve incompressible flow problems have undergone major improvements in the last few decades [1,2]. In this thesis we will discuss a new class of numerical approaches to solving one of the most common differential equations of physics, the Navier-Stokes equation of hydrodynamics. Hydrodynamics is chiefly interested in situations where different parts of a fluid move with respect to one another (and with respect to solid obstacles) at velocities that are much smaller then that of sound. The phenomenology of fluids can be enormously varied. Depending on the speed of the main flow, the size and shape of the obstacles, and the viscosity of the fluid, one can have purely laminar flow, vortices, turbulence, etc.

In this context, the relevant variable is the *velocity* $\mathbf{u}$ (a vector) of flow at different points, and the relevant parameter is the *viscosity* ν of the fluid. The behavior of the fluid is governed by the *Navier-Stokes* equation

$$\frac{\partial \mathbf{u}}{\partial t} + (\mathbf{u}\nabla)\mathbf{u} = -\frac{1}{\rho}\nabla p + \nu\nabla^2\mathbf{u} \tag{1.1}$$

where p is the pressure and ρ is the density. This is a nonlinear differential equation, and, except for special cases, one must make recourse to numerical methods in order to find its solution for given initial and boundary conditions.

An alternate approach to studying fluid flow properties (as opposed to solving the above equation) is the construction of models of fluids consistent with the Navier-Stokes equation. It turns out that models of fluid dynamics based on so called Cellular Automata have a number of attractive features and show considerable practical promise.

The term Cellular Automata, first introduced by von Neumann and Ulam in 1948, implies:

- dynamical variables defined at the nodes of a Lattice.
- dynamical variables taking values in a finite set
- synchronous application of a local transition rule at each lattice site, so that the new value of a dynamical variable at each site is a particular function of its current value and of the values of dynamical variables in a small neighborhood.

The class of cellular automata used for the simulation of fluid dynamics are called Lattice Gas Cellular Automata (LGCA). The algorithms are based on discrete lattice models of interacting "particles", whose *continuum description is governed by the equations of continuum fluid flow* (1.1). Point particles undergo displacements on a regular lattice in discrete time-steps with collisional processes represented by configurational transitions at lattice nodes. The LGCA have some advantages over conventional methods of solution of the Navier-Stokes equations in that they allow a considerable gain in computational efficiency and in some cases permit a deeper theoretical analysis.

However, it is not obvious that, on a macroscopic scale, the gases described by a cellular automaton rule obey the Navier-Stokes equation (1.1). It turns out that some of them *do not*, and those which do, show the fluid-like behavior only *approximately*.

The question must be raised as to the validity of the LGCA to represent actual fluids. The theoretical analysis of the lattice gas model does allow an answer to this question and can be carried out relatively easily. One views the lattice gas as a simplified version of the hard-sphere gas. Starting from exact micro-dynamical equations, statistical-mechanical computations can be conducted rather straightforwardly in a logical fashion with well controlled assumptions which bypass the many-body problem. The macroscopical parameters of LGCA can be then evaluated analytically . Results depend considerably on the model under consideration. We may find, for example, that in some models the discrete nature of LGCA affects the resulting "macro-dynamical equations" in the sense that the density and mass current may not be invariant under arbitrary rotations as is the fact in real fluids [3]. The other dis-

advantage is that practically all LGCA's have spurious conservation laws, as artifacts of the discrete space-time structure [3]. These spurious conservation laws will generate additional hydrodynamic equations containing spurious transport coefficients and hence should be carefully accounted for in the study of LGCA.

It turns out that all the macrodynamics depends considerably on the microscopic construction of particular cellular automaton. The essential point here is the existence of the conservation laws. Similarly to the situation in the theory of continuous fluids [4], momentum conservation is vital for the existence of a flow velocity and for sound waves. The macroscopic equation for energy balance is vital for problems involving convection. The theory of LGCA is general enough to include all desired conservation laws, although there are often spurious ones as well.

As mentioned, the theoretical analysis of LGCA is based on well known approximations in theory of liquids: the assumption of molecular chaos, the approximations of Chapman-Enskog analysis, linearizations of the collision matrix etc. The validity of these approximations is not obvious in LGCA models. Hence the special interest in "experimental" confirmation of the theory, namely computer simulation of LGCA. In such a simulation we investigate the density fluctuations. The motivation for this is that a fluid at global equilibrium can be viewed as a reservoir of excitations triggered by spontaneous fluctuations which temporarily disturb the system from local equilibrium. The excitations extend over a broad range of wavelengths and frequencies from the hydrodynamic scale down to the range of the intermolecular potential.

Non-intrusive scattering techniques are used to probe these fluctuations at the molecular level (neutron-scattering spectroscopy) and at the level of collective excitations (light-scattering spectroscopy). The quantity measured by these scattering methods is the power spectrum of density fluctuations, i.e., the dynamic structure factor $S(\mathbf{k},\omega)$ which is the space and time Fourier transform of the correlation function of the density fluctuations. The spectral function $S(\mathbf{k},\omega)$ describes the dynamical behavior of spontaneous fluctuations and it illustrates how the details of the microscopic processes manifest themselves at the macroscopic level. The most obvious

such manifestation is the description of the transport coefficients. While water and molasses both satisfy the Navier -Stokes equations, they do so with very different viscosities and diffusivities. All those differences show up in the form of the dynamic structure factor (as will be shown in Section 1.8). Thus the "fluid-like" form of the Structure Factor which results from computer simulation can be treated as a criteria for the success of a particular LGCA model. During the simulation other theoretical results can also be tested unambiguously.

1.1.1 Outline of later chapters

Chapter 1 begins with a review of lattice gas theory, and establishes notation that is used throughout the rest of the thesis. The main foci of this chapter are the Boltzmann evaluation of transport coefficients and the general derivation of the Landau-Placzek expression for the dynamic structure factor of a LGCA.

Chapter 2 contains a simple example of a LGCA model with detailed analysis from both the theoretical and the computational point of view. We analyze the structure factor and transport properties of the model and compare simulation results to the known results for continuum fluids.

In the Chapter 3 we introduce the relatively complicated *thermal* LGCA. Consistency with classical equilibrium thermodynamics is given a special attention. Several results of computer simulations are presented to demonstrate some essential features for the construction of useful LGCA models. The results confirm that thermal Lattice Gas Automata are consistent models for real fluids.

Finally, in the last Chapter, we summarize the results presented in this thesis and discuss the advantages and disadvantages of the various models.

1.2 General definitions and notation

A lattice gas is generally described by a state space and by a time-development rule. The state space is defined by associating b possible states for particles at each point of a lattice L (we will in future refer to these lattice points as lattice *sites*). At each site there can be many particles, but only *one* in each of the possible states. Each state is associated with the velocity of a particle residing at the given site of lattice (hence we often refer to the states as *velocity channels*). This arrangement allows us to associate each state on a given site with one *bit*, (bits are Boolean variables taking the values 0 or 1), and the particle configuration of the site with one b-word. Particular LGCA models are thus often referred to as b-bit lattice gas models.

We denote the total number of bits on the lattice by $N = b|L|$. For each value of the discrete time parameter t, we write the values of the bits as $n_i(\mathbf{r}, t)$, where the discrete vector $\mathbf{r} \in L$ counts all the sites of lattice and i counts the bits at lattice site $\mathbf{r}$ or, equivalently, enumerates the states of the particles (or velocity channels) at this site. We interpret the function $n_i(\mathbf{r}, t)$ as an *occupation number* since it gives the value of the particle number of each velocity channel. This value is either 1 or 0, namely the particle in the given state is either present or absent. So the particles obey the *Fermi exclusion rule* and hence all the statistical description of LGCA is similar to that of the Fermi gas, as will be shown in Section 1.6.

Since the finite set of states directly corresponds to the finite set of particle velocities, the number of all states b for a given model is defined by the symmetry of the underlying lattice, namely the number of nearest neighbors for any given site and by a restriction on the absolute value of the velocity, namely that allowed velocities connect the site with its nearest neighbors, next nearest neighbors, etc. *Rest particles*, having $\mathbf{c} = 0$, are also allowed in certain models. We denote the discrete set of velocity vectors by $\mathbf{c}_i, i = \{1, ..., b\}$, hence the set of velocity vectors coincides with a set of all possible displacements of particles residing at a given site.

Now we consider the time evolution of LGCA. This process consists of a *collision*

step and a *propagation step*. The collisions are local, and occur simultaneously at each site at equal time intervals Δt according to particular rules defined for each model. Collision rules are often conveniently represented by a *collision table*: a list of diagrams depicting all possible *precollisional states* at a site with the corresponding *postcollisional* state(s). In such a diagram the presence of particle with velocity $\mathbf{c}_i$ is marked by an arrow with the corresponding direction and length. Figures 2.2 and 3.2 of this thesis are examples of collision tables. Collisions are then followed by the propagation of particles. Each particle moves to another site according to the value of its velocity, so that the value of bit i at site $\mathbf{r}$ becomes that of bit i at site $\mathbf{r}+\mathbf{c}_i\Delta t$. This can also be viewed as a change from the postcollisional state at time t to the precollisional state at time $t+\Delta t$.

Finally, it is worth mention that the boolean nature of the occupation numbers is the main feature which allows effective numerical simulation with remarkable computational efficiency. The state of the system in such a simulation is represented by a matrix of $\mid L \mid$ b-bit-words, each of them describing the state of a site. In this representation, the propagation step of the dynamics consist in moving bits from each matrix element to adjacent ones: an operation particularly suited to massively parallel computer hardware.

1.3 Microscopic dynamical equation

As already described, for each value of $i \in \{1, \ldots, b\}$ there is a lattice vector $\mathbf{c}_i$ such that $\mathbf{r} + \mathbf{c}_i \Delta t \in L$ for every $\mathbf{r} \in L$ where Δt is the duration of one time-step. It is convenient to set Δt equal to unity.

We wish to express the evolution of LGCA in the form of an equation for the microscopic dynamics of the lattice gas; that is, we desire an equation for $n_i(\mathbf{r}, t+1)$ in terms of $n_i(\mathbf{r}, t)$, where Δt denotes the timestep. Suppose, for a moment, that the particles simply propagated without colliding. Then the dynamics would be described by the following free streaming equation:

$$n_i(\mathbf{r} + \mathbf{c}_i, t+1) = n_i(\mathbf{r}, t).$$

The addition of collisions introduces a *collision operator* on the right-hand side of the above equation. That is, we have

$$n_i(\mathbf{r} + \mathbf{c}_i, t+1) = n_i(\mathbf{r}, t) + \Omega_i\left(n_*(\mathbf{r}, t)\right), \tag{1.2}$$

where the collision operator, Ω_i, describes the change in bit i due to collisions and is a nonlinear function of a limited set of occupation numbers $n_*(\mathbf{r}, t)$ in the small neighborhood of a given node $\mathbf{r}$. In other words, the collision operator depends on the occupation function n for all possible values of the index represented by the asterisk. All terms in the collision operator are the products of occupation numbers of particles $n_i(\mathbf{r}, t)$ or "holes" $\bar{n}(\mathbf{r}, t) = 1 - n_i(\mathbf{r}, t)$ at the lattice site where the collision took place. The factors $\bar{n}$ ensure that multiple collisions can only occur if the appropriate post-collisional states are empty or occupied by "holes". This is a consequence of the Fermi exclusion rule. In general, the collision process at a fixed lattice site and timestep can be fully specified by a 2^n by 2^n *transition matrix* A, whose element $A(s \rightarrow s')$ is unity if and only if the particles in state $s = \{n_i(.) = 0 \text{ or } 1, i = 1, \ldots b\}$ collide to yield particles in state s'. Since each incoming state gives rise to exactly one outgoing state,

$$\sum_{s'} A(s \rightarrow s') = 1. \tag{1.3}$$

The relationship of this matrix to the collision operator Ω will be shown in Section 1.7.

It is worth stressing the big variety of possibilities for constructing the collision matrix (collision rules) even under the restriction of conservation laws for any fixed d-dimensional lattice. The way we choose the collision matrix defines the model itself and affects its macroscopic properties in general. For an example of the construction of the collision term in Eq.(1.2) for a particular model see Section 2.2.

Often, however, precise knowledge of each and every bit of the system is more information then one really desires. So we now consider some statistical aspects of lattice gas theory. Let us suppose that we have prepared an ensemble of lattice gas simulations, on grids of the same size, with different initial conditions. We may then take averages across this ensemble. We shall denote these ensemble averages by angular brackets $\langle\rangle$. But we denote the ensemble average of the quantity $n_i(\mathbf{r},t)$ by $f_i(\mathbf{r},t)$; that is

$$f_i(\mathbf{r},t) = \langle n_i(\mathbf{r},t)\rangle \tag{1.4}$$

Note that while the n_i's are binary, the f_i's have values in the set of real numbers between zero and one. Physically $f_i(\mathbf{r},t)$ gives the probability of finding a particle with velocity $\mathbf{c}_i$ at position $\mathbf{r}$ at time t, averaged over configurations.

Similarly we define the matrix of transition probabilities $A_{ss'}$:

$$A_{ss'} = \langle A(s \to s')\rangle \tag{1.5}$$

A coarser description, such as a closed set of kinetic equations for the one-particle distribution function defined in (1.4) is then a more appropriate description of the system. In this description we expect to get the hydrodynamical behavior of the system.

The idea that macroscopic properties of a physical system should be independent of the microscopic definition of the system is also a familiar concept in equilibrium statistical mechanics and in quantum field theory. In such theories, the effect of looking at the physics of the system at larger and larger scales is mathematically

described by the renormalization group flow of the system [5]. Generally, as the scale of the physics of interest becomes extremely large compared to the scale at which the system is defined, one finds that the renormalization group flow takes the system towards certain fixed points, which describe entire universality classes of theories with identical macroscopic behavior. The emergence of similar hydrodynamic equations in a variety of systems with different microscopic dynamics is an equivalent phenomenon in nonequilibrium statistical mechanics.

1.4 Conserved quantities

A distinguishing feature of lattice gases is the presence of some number of conserved quantities that are linear in the bit values. The presence of conserved quantities is the key argument in understanding why we should expect the bulk behavior of particles moving and colliding on a lattice to be that of a fluid. In nature we observe that many different fluids, with drastically differing intermolecular force laws, all satisfy the Navier-Stokes equations to a reasonable degree of approximation. In spite of all the differences between the intermolecular collisions in, say, water and molasses, both conserve mass and momentum; ultimately the existence of these conserved quantities when combined with other conditions discussed later is what gives rise to fluid-like behavior at the macroscopic level [6]. On a more theoretical level conserved quantities ensure the existence of respective conjugate thermodynamic variables and the existence of an equilibrium state of the fluid corresponding to these quantities.

The quantities that are conserved may differ from one LGCA model to another. For example, in some lattice gases, the total number of particles is a conserved quantity; it is clearly conserved by the propagation phase of the timestep, and we can choose collision rules that conserve the particle number as well. Let us assume that we have a lattice gas with some number of conserved quantities with corresponding densities, such as

$$\textit{number of particles} \qquad \rho(\mathbf{r},t) = \sum_i n_i(\mathbf{r},t) \tag{1.6}$$

$$\textit{momentum} \qquad \mathbf{g}(\mathbf{r},t) = \sum_i \mathbf{c}_i n_i(\mathbf{r},t) \tag{1.7}$$

$$\textit{energy} \qquad \varepsilon(\mathbf{r},t) = \sum_i \frac{1}{2} c_i^2 n_i(\mathbf{r},t) \tag{1.8}$$

More explicitly the total number of particles $N = \sum_{\mathbf{r}} \rho(\mathbf{r},t)$, the total momentum of the system $P = \sum_{\mathbf{r}} \mathbf{g}(\mathbf{r},t)$ and the total energy $H = \sum_{\mathbf{r}} \varepsilon(\mathbf{r},t)$ are constants of the motion.

Because the corresponding densities can change only through free streaming but

not through collisions the collision term in Eq.(1.2) must satisfy the relation:

$$\sum_i q(c_i)\Omega_i\left(n_*(\mathbf{r},t)\right) = 0 \tag{1.9}$$

where $q(c_i) = \{1, \mathbf{c}_i, \frac{1}{2}c_i^2, ...\}$. From (1.2) the local microscopic conservation laws then take the form

$$\sum_i q(c_i)[n_i(\mathbf{r}+\mathbf{c}_i, t+1) - n_i(\mathbf{r},t)] = 0 \tag{1.10}$$

In terms of introduced in previous section ensemble average we can thus consider averaged values of the conserved quantities (1.6)-(1.8)

$$Q = \langle Q(\mathbf{r},t)\rangle = \langle \sum_i q(c_i)n_i(\mathbf{r},t)\rangle = \sum_i q(c_i)f_i(\mathbf{r},t) = N, P, H, ... \tag{1.11}$$

where the average is calculated with the local equilibrium distribution. In terms of matrix of transition probabilities (1.5) the conservation laws take the form

$$A_{ss'}h(s) = A_{ss'}h(s') \tag{1.12}$$

$$h(s) = \sum_i q(c_i)n_i(.) \tag{1.13}$$

No summation over repeated indexes is implied. Physically Eq.(1.12) implies that if the transition occurs ($A_{ss'} \neq 0$) then the value $h(s) = \sum_i q(c_i)n_i(.)$ of the conserved quantity in the pre-collisional state s is equal to that in the post-collisional state s'.

We observe in passing that some lattice gases also posses *spurious global conserved quantities*. Such spurious global conserved quantities have no analog for continuum fluids, and need to be considered carefully when using lattice gases to model hydrodynamic phenomena. (See, e.g., [7–9].) For example, the most frequently occuring spurious invariant is the total staggered momentum [10,11]. The existence of this invariant can be easily understood by using a trivial one-dimensional example. Let $g(x)$ be the linear momentum of the particles present at site x. Define

$$G_e(t) = \sum_{x\,even} g(x,t) \tag{1.14}$$

$$G_o(t) = \sum_{x\,odd} g(x,t)$$

as the total momentum of the particles on even or odd sites and let the collision rules conserve the momentum and the number of particles at each site. If we choose also that the particles can only hop between nearest neighbors, then G_e and G_o are exchanged at each time step. Due to this extremely simplified dynamics a new conserved quantity $S = (-1)^t(G_e - G_o)$, called the staggered momentum, is present in addition to the usual total number of particles N and the total linear momentum $G_e + G_o$. Similar staggered conserved quantities exist in higher dimensional models. For example, lattice gases of single-speed particles on a Cartesian grid conserve some quantities separately on both checkerboard sublattices [7,8]. These models are usually insufficiently symmetric [3] and do not seem to have any interesting applications.

In Sec.2.1 we encounter also the unwanted conservation of the particle number difference between any pair of opposite directions for a specific FHP model. As was shown in a number of papers [11,12], the existence of spurious invariants leads to modified hydrodynamics which is strongly tied to the microscopic structure of the model. It is therefore important to consider models where the presence of spurious invariants is eliminated or minimized. For example, the staggered momentum of the above example on the linear lattice can easily be destroyed by allowing for next-nearest neighbor hops.

Finally we note that LGCA may not conserve energy. If energy is conserved, one has a *thermal* lattice gas model in which temperature can be defined in accord with thermodynamics, (see Section 1.6 for details). If the energy is not conserved or is simply a multiple of the particle density, such as in the simple FHP model discussed in Chapter 2, one has an *athermal* lattice gas model.

1.5 The Boltzmann Equation

To obtain a closed set of equations for the f_i, we take the ensemble average of Eq. (1.2). We are immediately confronted by the fact that the collision operator is generally a nonlinear function of the occupation numbers n_i. As is well known, the average of a nonlinear function of a set of variables is not in general expressible as a function of the averaged variables. It also depends on the *correlations* between the quantities – in this case on those between the incoming bits, n_i.

Thus, the simplest approximation that we can make to close the system of equations for the f_i is to assume that the incoming bits, n_i, are uncorrelated. This is the discrete version of the famous *Boltzmann molecular chaos assumption.* From this assumption, it follows that

$$\langle \Omega_i(n_*) \rangle \approx \Omega_i(\langle n_* \rangle) = \Omega_i(f_*),$$

In this way, we get the *lattice Boltzmann equation*,

$$f_i(\mathbf{r} + \mathbf{c}_i \Delta t, t+1) = f_i(\mathbf{r}, t) + \Omega_i\left(f_*(\mathbf{r}, t)\right). \tag{1.15}$$

Physically speaking, the assumption of molecular chaos supposes that the propagation substep effectively decorrelates the different bits at each site[1]. That is, it supposes that colliding particles have never had any prior effect on each other. This assumption is almost never strictly correct for a system of particles moving on a discrete lattice in a finite number of dimensions. By standard combinatorial arguments, the reencounter probability for two particles executing a random walk on a lattice is unity in one and two dimensions, is less than unity in three or more dimensions, and falls to zero as the number of dimensions goes to infinity. One might thus expect that the molecular chaos assumption becomes more valid as the number of spatial dimensions increases. Indeed, this is the case, and the molecular chaos assumption can be thought of as a sort of mean-field theory. In addition, in some circumstances,

[1]For stochastic lattice gases, such decorrelation is enhanced by the injection of stochasticity at each site at each time step.

it is possible for particles to set up coherent structures that persist for long times. Such structures, by their very nature, invalidate the molecular chaos assumption in a rather dramatic way. LGCA models with this characteristic are clearly not good models for fluid motion.

1.6 Thermodynamics

Non-equilibrium fluid dynamics is of great practical interest in the physics of liquids. In many cases the non-equilibrium state of the fluid (or the LGCA) can be visualized as a collection of local equilibria that smoothly merge into one another and smoothly evolve in time; the various macroscopic quantities *flow* in a continuous way.

This is because in a very large system, even relatively small portions of the system still contain a large number of parts, and thus can be meaningfully subjected to a macroscopic analysis. The equilibrium has established itself on a certain scale, so that the system as a whole is not at equilibrium. In this situation, the macroscopic parameters gradually change from place to place; moreover, at each place these parameters may gradually change also in time - such macroscopic evolution being of course driven by the spatial gradients of the macroscopic quantities involved. Because in this scheme the existence of thermodynamic equilibrium is essential we next consider the thermodynamics of the equilibrium state of LGCA.

Let us assume that, given any initial conditions, the lattice gas evolves in such a way that it eventually attains some sort of *steady state*. This is achieved when particles travel and collide with one another. Collisions lead to a gradual *randomization* of the particles' paths. This implies that, regardless of the initial distribution of particles, but after a certain amount of time for evolution, the system at any given time-step looks just as random as it looked one or more time-steps before; in physical terms, the entropy will not decrease. The lattice gas then effectively displays irreversible behavior.

We should mention here the special class of LGCA where, during evolution, each microscopic particle configuration has its unique predecessor state as well as its unique successor. These lattice gas models are called *deterministic* as opposed to *nondeterministic* models, where each microscopic configuration has several possible outcomes, each of them weighted with some probability. Here we approach one of the central questions of statistical mechanics regarding reversibility: *How do we get randomiza-*

tion if the collision rules are usually chosen to be microscopically reversible ? Or in other words, why we should expect the deterministic model to be reversible? The rules for collisions on each site thus correspond to a simple permutation of the possible particle arrangements. Hence the evolution of a complete particle configuration can be reversed by applying inverse collision rules at each site. The discrete nature of the cellular automaton model makes such precise reversal in principle possible. But the rapid randomization of microscopic particle configuration implies that very complete knowledge of the current configuration is needed. With only partial information, the evolution may be effectively irreversible.

The macroscopic irreversibility and the existence of a steady state do not ensure that we can use the methods of Classical Thermodynamics and Statistical Mechanics. The essential condition here is the existence of a *universal equilibrium state* which depends only on macroscopic conserved quantities. It turns out that not every cellular automaton rule leads the LGCA to universal equilibrium. In order to understand when the steady state is at the same time a universal equilibrium state, we describe the time evolution of the LGCA in terms of a probability distribution function $P(s,t)$ denoting the probability that the dynamic variables $n_i(\mathbf{r},t)$ take the values corresponding to the state s. This way one arrives at the Liouville equation of stochastic dynamics which is analogous to the microdynamic equation for deterministic dynamics, see [13]:

$$P(t+1) = S^{-1}AP(t) \tag{1.16}$$

with A being the matrix of transition probabilities as in (1.5). S is the streaming operator, mapping the post-collision state $\mathbf{r}, \mathbf{c}_i$ at time t to the pre-collision state $\mathbf{r}+\mathbf{c}_i, \mathbf{c}_i$ at time $t+1$. The equilibrium solution in the long time limit of the probability distribution of occupation numbers $\rho_0(s) = \lim_{t\to\infty} P(t)$ satisfies:

$$S^{-1}A\rho_0(s) = \rho_0(s) \tag{1.17}$$

This is a mathematical representation of the physical definition of the equilibrium. The equilibrium distribution does not change under the action of either streaming or

collision operators and this places conditions upon the collision matrix A.

To see them we assume that there exists an universal equilibrium solution $\rho_0(s) = D(Q(s))$, depending on the configuration only through the globally conserved quantities $Q(s)$ defined in (1.11). We separately consider the action of the free streaming operator S and the collision operator A. As $Q(s)$ is a sum of single particle quantities, and as the system obeys periodic boundary conditions, $Q(s)$ and $D(Q(s))$ are invariant under free streaming. To obey the Liouville equation, $D(Q(s))$ should therefore satisfy $D = AD$ or

$$D(Q(s)) = \sum_{\sigma} A_{s\sigma} D(Q(s)) \tag{1.18}$$

On account of (1.12) this reduces to the *semi-detailed balance condition*,

$$\sum_{s} A_{\sigma s} = 1 \tag{1.19}$$

We derived this condition from the assumption of the existence of a statistical equilibrium solution defined only by the values of the macroscopic conserved quantities Q. So if the semi-detailed balance condition is not satisfied, the equilibrium distributions are not simply function of the invariants Q, and depend explicitly on the transition rules. This class of models does not have much physical interest and will not be considered further. We note that the LGCA considered in this thesis obey the even stronger condition of *detailed balance*

$$A_{\sigma s} = A_{s\sigma} \tag{1.20}$$

requiring that the forward and backward collision rates be equal. On account of (1.3) this satisfies the semi-detailed balance condition (1.19).

1.6.1 Boltzmann Equilibrium

The statistical mechanics of the LGCA universal equilibrium state is conveniently described by a grand ensemble [14] with a phase space density proportional to $exp(\mathbf{bQ})$ [15] where Q as defined by (1.11) includes all spurious invariants, and all physical

ones. The set of thermodynamic fields $\mathbf{b}(\mathbf{r},t)$ includes the chemical potential $\mu(\mathbf{r},t)$, the reciprocal thermodynamic temperature $\beta(\mathbf{r},t)$ and conjugates to the momentum $\gamma(\mathbf{r},t)$ and to spurious conserved quantities $\mathbf{b}_s(\mathbf{r},t)$. They are conjugate to the *average* or *macroscopic* densities $Q(\mathbf{r},t)$, defined in (1.11).

By setting $\gamma = 0$, (and if necessary setting all spurious conjugate thermodynamic variables to zero), one ensures that $\langle \sum_i c_i n_i(\mathbf{r},t) \rangle = P = 0$, so that the lattice gas is macroscopically at rest. The ensemble then reduces to the grand canonical ensemble so that we can write the probability distribution of occupation numbers in statistical equilibrium $\rho_0(s)$ as:

$$\rho_0(s) = C exp[\mu N - \beta H] \tag{1.21}$$

where $C = C(\mathbf{b})$ is the grand partition function or normalization factor to ensure the ensemble density is normalized to unity [14]:

$$C = \sum_N {\sum_s}' e^{-[\sum_{\mathbf{r},i}(\mu - \frac{1}{2}\beta c_i^2) n_i(\mathbf{r},t)]} \tag{1.22}$$

The prime indicates that the summation over occupation numbers is constrained to situations with exactly N particles. We note that the summand does not contain a factor $\frac{1}{N!}$ because the particles are indistinguishable.

Since the numbers $n_i(\mathbf{r},t)$ can be either 0 or 1, the further analysis is exactly the same as in the statistical mechanics of the Fermi gas (see, for example, [15]). In particular the mean occupation number of a single-particle state is given by

$$f_i^0 = \langle n_i(\mathbf{r},t) \rangle = \frac{1}{C}\left[-\frac{1}{\beta}\left(\frac{\partial C}{\partial \epsilon}\right)_{\mu,\beta}\right] = \frac{1}{1 + \exp\left(-\mu + \beta\frac{1}{2}c_i^2\right)}, \tag{1.23}$$

where $\epsilon = \frac{1}{2}c_j^2$ is the kinetic energy and $f_i^0 = lim_{t\to\infty} f_i(t)$ is the longtime limit of the probability function f (1.4), which is invariant under the Boltzmann equation (1.15). For this reason, the equilibrium is often referred to as *Boltzmann equilibrium*. If the Boltzmann equilibrium is spatially uniform, it can be specified by a set of values for the n mean occupation numbers, f_i; and the associated distribution on the set of states is given by independently sampling each bit n_i with probability f_i.

In general the Boltzmann distribution of the model with an arbitrary set of conserved quantities $q_\lambda(c_i)$ is given by

$$f_i^0 = \frac{1}{1 + e^{-\sum_\lambda b_\lambda q_\lambda(c_i)}} \tag{1.24}$$

where the set b_λ are conjugate to the invariants q_λ.

1.6.2 Thermodynamic quantities and relations

In terms of the distribution function (1.23) we can write explicit expressions for the basic thermodynamic quantities which have the same form as in the ideal Fermi gas except that the sum over velocities is restricted to a small set of b values:

$$N = \rho V = -\partial lnC/\partial\mu = V\sum_i f_i^0 \tag{1.25}$$

$$H = \epsilon V = \partial lnC/\partial\beta = V\sum_i \frac{1}{2}c_i^2 f_i^0 \tag{1.26}$$

$$S = -\langle ln\rho(s)\rangle = \sum f_i^0 ln f_i^0 + (1 - f_i^0)ln(1 - f_i^0) \tag{1.27}$$

$$PV\beta = lnC = -V\sum_i ln(1 - f_i^0) \tag{1.28}$$

where N is the total number of particles, H the total energy, C is defined by (1.22) and S is the entropy. Equation (1.28) defines the thermodynamic pressure of a lattice gas. However, in the literature [14] one often uses the kinetic pressure which is defined through the virial theorem, or through the momentum flux density

$$p_K = \sum_i c_x^2 f_i^0 = \frac{2}{d}\epsilon = \frac{2}{d}\sum_i \frac{1}{2}c_i^2 n_i(\mathbf{r}, t) \tag{1.29}$$

A kinetic temperature is sometimes also introduced [16] through the relation $p_K = \rho k_B T$. This temperature is of course different from the thermodynamic temperature, as was shown in [14]. The introduction of the kinetic pressure and the kinetic temperature is justified by the simplicity arising from their linear dependence on the occupation numbers. In the limit of low densities $f_i^0 \to 0$ and high temperatures $\beta \to 0$ the kinetic and thermodynamic pressures become equivalent, because

$$p = -\frac{1}{\beta}\sum_i ln(1 - f_i^0) \Rightarrow \epsilon\sum_i f_i^0 = p_k \tag{1.30}$$

In last equality we used the fact that in the high temperature limit, the f_i^0 do not depend on i and can be taken out of the summation in Eq.(1.29).

An important property of lattice gases is the speed of sound defined as

$$c_s = [(\frac{\partial p}{\partial \rho})_S]^{\frac{1}{2}} \tag{1.31}$$

where S is the entropy per particle (1.28). It can be easily evaluated using linear response, which relates the fluctuation in a given quantity to thermodynamic derivatives [17]. This allows us to write:

$$T(\frac{\partial \langle n_i \rangle}{\partial \mu})_S = \langle (\delta n_i)^2 \rangle \tag{1.32}$$

$$-T(\frac{\partial \rho}{\partial V})_S = \langle \delta p \delta \rho \rangle \tag{1.33}$$

$$-T(\frac{\partial p}{\partial V})_S = \langle (\delta p)^2 \rangle \tag{1.34}$$

so that

$$c_s^2 = (\frac{\partial p}{\partial V})/(\frac{\partial \rho}{\partial V}) = \frac{\langle (\delta p)^2 \rangle}{\langle \delta p \delta \rho \rangle} = \frac{\sum_i c_i^4 \langle (\delta n_i)^2 \rangle}{d \sum_i c_i^2 \langle (\delta n_i)^2 \rangle} \tag{1.35}$$

In the last equation we used the definition of kinetic pressure (1.29). To obtain the fluctuation of $\delta n_i(\mathbf{r}, t)$ we differentiate the Fermi-Dirac distribution (1.23) with respect to the chemical potential μ

$$\langle \delta n_i(\mathbf{r}, t) \delta n_{i'}(\mathbf{r}', t) \rangle = k_i \delta_{i,i'} \delta_{r,r'}$$

$$k_i = f_i^0 (1 - f_i^0) \tag{1.36}$$

The delta-functions come from the fact that there are no spatial correlations in a lattice gas.

Combining Eqs.(1.36) and (1.36) we find for the velocity of sound:

$$c_s^2 = \frac{\sum_i k_i c_i^4}{d \sum_i k_i c_i^2} \tag{1.37}$$

1.7 Linear approximation to the Boltzmann equation

As mentioned in Section 1.6 the most interesting physics of fluids appears when the system is driven away from its equilibrium state. The response of the system to an external perturbation is known to be related to transport phenomena and will be discussed in Section 1.9 of this chapter. The lattice Boltzmann equation (1.15) fully describes the LGCA out of equilibrium, but, because of the nonlinearity and complexity of the collision operator is of little practical use in the evaluation of transport coefficients. Here we consider a linear approximation to the Boltzmann transport equation.

This approach assumes that the distribution function f_i differs only slightly from the equilibrium form f_i^0 (1.23). Thus we can make an approximation:

$$f_i = f_i^0 + \Phi_i \qquad (\frac{\mid \Phi_i \mid}{f_i^0} \ll 1) \tag{1.38}$$

With this approximation the collision term Ω_i in the Boltzmann transport equation may be approximated by a power series expansion in Φ_i

$$\Omega_i = \sum_j \Omega_{ij}^{(1)} \Phi_j + \sum_{jk} \Omega_{ijk}^{(2)} \Phi_j \Phi_k + ... \tag{1.39}$$

where $\Omega^{(1)}$ is the linearized collision operator. Notice that for a model with collisions involving at most K particles, the expansion (1.39) terminates at $O(\Phi^K)$. As was shown in Refs.[6,12] the linearized collision operator $\Omega^{(1)}$ can be expressed in terms of the matrix of transition probabilities (1.5)

$$\Omega_{ij}^{(1)} k_j = \sum_{ss'} (s_i - s_i') A_{ss'} \rho_0(s) s_j \tag{1.40}$$

where $\rho_0(s)$ is the probability distribution of occupation numbers given by (1.21). We further observe that the product matrix

$$(\Omega^{(1)} k)_{ij} = \Omega_{ij}^{(1)} k_j \tag{1.41}$$

is symmetric for models obeying detailed balance (1.20). The matrix $\Omega^{(1)}$ is in general non-symmetric. However in the special case of one-speed models this matrix becomes symmetric because k_i does not depend on the subscript i. In such athermal models the conservation laws (1.10) written in terms of the microscopic collision operator (1.2) yield conditions on all the $\Omega^{(n)}$ of the form:

$$\sum_{ijk\ldots} \Omega^{(n)}_{ijk\ldots} = 0$$
$$\sum_{ijk\ldots} c_i \Omega^{(n)}_{ijk\ldots} = 0 \tag{1.42}$$

In a spatially uniform system close to equilibrium one may use a linear approximation to the Boltzmann equation

$$f_i(\mathbf{r}+\mathbf{c}_i, t+1) - f_i(\mathbf{r}, t) = \sum_j \Omega^{(1)}_{ij} \Phi_j \tag{1.43}$$

This equation can be solved in terms of the eigenvalues α_λ and eigenvectors Ψ_λ of the matrix $\Omega^{(1)}$ *i.e.*,

$$\Omega^{(1)} k_i \Psi_\lambda = \alpha_\lambda k_i \Psi_\lambda \tag{1.44}$$

with eigenvalues satisfying the inequalities,

$$0 \leq -\alpha_\lambda < 2 \tag{1.45}$$

(see Sec.1.8 for justification). The inclusion of k_i as defined in (1.36) is convenient because it defines the eigenfunctions Ψ_λ to be orthogonal with respect to a *weighted thermal inner product*

$$< \Psi_\lambda \mid \Psi_m > = \sum_i k_i \Psi_\lambda(c_i) \Psi_m(c_i) = \delta_{\lambda m} \tag{1.46}$$

The Φ_i may always be written [18] as sums of pieces proportional to each of the orthogonal eigenvectors Ψ_λ

$$\Phi_i = \sum_\lambda B_\lambda \Psi_\lambda(c_i) \tag{1.47}$$

and the general solution of Eq.(1.43) is given in terms of Eq.(1.47) by

$$B_\lambda(t) = B_\lambda(0) e^{\alpha_\lambda t} \tag{1.48}$$

Since all nonzero α_λ have negative real parts, the associated B_λ must decay exponentially with time. Only the combinations of Φ_i associated with zero eigenvalues survive at large times.

It is easy to show that the set of eigenfunctions Ψ_λ with zero eigenvalues is proportional to the set of conserved quantities $q_\lambda(c_i) = \{1, \mathbf{c}_i, \frac{1}{2}c_i^2, ...\}$ defined in (1.9). Since $\Omega_i(f^0(b_\lambda)) = 0$ for any set of b_λ conjugate to the conserved quantities q_λ (1.24), it follows that

$$\sum_j \frac{\partial \Omega_i}{\partial b_\lambda} = \sum_j \frac{\partial \Omega_i}{\partial f_j}\frac{f_j}{\partial b_j} = 0 \tag{1.49}$$

However, the derivative $\frac{\partial \Omega_i}{\partial f_j}$ is just $\Omega_{ij}^{(1)}$, and so writing the derivatives $\frac{\partial f_j}{\partial b_\lambda}$ explicitly, we obtain

$$\sum_j \Omega_{ij}^{(1)} \frac{df_j^0}{db_\lambda} = \sum_j \Omega_{ij}^{(1)} k_j q_\lambda(\mathbf{c}_j) = 0 \tag{1.50}$$

showing that the $q_\lambda(c_j)$ are indeed eigenvectors of $\Omega_{ij}^{(1)}$ with zero eigenvalues. Hence corresponding eigenvectors with zero eigenvalue play a special role and are associated with the conservation laws (1.10).

This result supports the local equilibrium assumption used for the derivation of hydrodynamic equations. It implies that regardless of the initial average densities Φ_i, collisions bring the system to an equilibrium that depends only on the values of the macroscopic conserved quantities.

1.8 Dynamic Structure Factor

In this section we introduce the formal definition and general properties of a time-correlation function, namely the dynamic structure factor, and thus establish the link between spontaneous time-dependent fluctuations and the response of a lattice gas to an external probe. The importance of density fluctuations in LGCA models lies in the first place in the fact that LGCA fluctuations as well as those in real fluids can be measured with a high degree of accuracy using computer simulations and light scattering experiments respectively [4]. Thus the value of LGCA as a model of a real fluid can be easily seen.

The Dynamic Structure Factor $S(\mathbf{k},\omega)$ is defined as the double Fourier transform with respect to space and time of the correlation function of density fluctuation $\delta\rho(\mathbf{r},t)$ around the equilibrium state:

$$\rho S(\mathbf{k},\omega) = \sum_{\mathbf{r}} \sum_{t=-\infty}^{\infty} e^{-i\omega t - i\mathbf{k}\cdot\mathbf{r}} < \delta\rho(\mathbf{r},\mid t \mid)\delta\rho(0,0) >= \sum_{t=-\infty}^{\infty} e^{-i\omega t} V^{-1} < \delta\rho(\mathbf{k},\mid t \mid)\delta\rho^{*}(0,0) > \tag{1.51}$$

where $\rho(\mathbf{k}) = \sum_{\mathbf{r}} exp(-i\mathbf{k}\cdot\mathbf{r})\rho(\mathbf{r})$ is the spatial Fourier transform of the density and $V =\mid L \mid = l^d$ is the number of nodes in the d-dimensional lattice.

The Fourier transformation of the linearized lattice-gas Boltzmann equation (1.43) yields to first order in the fluctuation δn_j:

$$\delta n_i(\mathbf{k},t+1) = \sum_j e^{-i\mathbf{k}\cdot\mathbf{c}_i}(\delta_{ij} + \Omega^{(1)}_{ij})\delta n_i(\mathbf{k},t) \tag{1.52}$$

Hence we can write the most important quantity in the non-equilibrium description of LGCA, namely the kinetic propagator Γ , as:

$$\Gamma_{ij}(\mathbf{r},t)k_j =< \delta n_i(\mathbf{k},t)\delta n^{*}_j(\mathbf{k},0) >= [e^{-i\mathbf{k}\cdot\mathbf{c}}(1+\Omega^{(1)})]^t_{ij}k_j \tag{1.53}$$

where k_j is the equal-time correlation function of the δn_i's given by (1.36). This form of the kinetic propagator as the t-th power of $e^{-i\mathbf{k}\cdot\mathbf{c}}(1+\Omega^{(1)})$ immediately implies that the eigenvalues of the matrix $(1+\Omega^{(1)})$ must have modulus < 1. This justifies the inequality (1.45) for the eigenvalues of the linear collision matrix.

Then summing Eq.(1.53) over (i,j) and taking the temporal Fourier transform yields the dynamic structure factor (1.52)

$$\rho S(\mathbf{k},\omega) = 2Re\sum_{i,j}\left\{\frac{1}{e^{i\omega+\mathbf{k}\cdot\mathbf{c}}-1-\Omega^{(1)}}+\frac{1}{2}\right\}_{ij}k_j \tag{1.54}$$

This is the expression for the dynamic structure factor in Boltzmann approximation. In general it is too complicated to be expressed analytically. However, when one is interested in the dynamic structure factor in the hydrodynamic regime, then the method of Landau and Placzek [19] allows the calculation of $S(\mathbf{k},\omega)$ analytically, from (1.54) in the limit of $\mathbf{k}\to 0, \omega\to 0$.

Equation (1.53) contains the t-th power of the non-symmetric matrix $e^{-i\mathbf{k}\cdot\mathbf{c}}(1+\Omega^{(1)})$. In matrix notation its right eigenvectors are defined through

$$e^{-i\mathbf{k}\cdot\mathbf{c}}(\mathbf{1}+\Omega^{(1)})\mid\Psi_\lambda(\mathbf{k})\rangle = e^{z_\lambda(\mathbf{k})}\mid\Psi_\lambda(\mathbf{k})\rangle \tag{1.55}$$

where the vector $\mid\Psi_\lambda\rangle$ has components $\mid\Psi_\lambda\rangle_i = k_i\Psi_\lambda(\mathbf{c}_i)$ with $i=1,2,...,b$.

First we note that in the $k\to 0$ limit this equation becomes essentially the same as Eq.(1.44) with

$$z_\lambda(\mathbf{k})\big|_{(k=0)} = ln(1+\alpha_\lambda) \tag{1.56}$$

We now can distinguish two types of eigenvalues or eigen-modes. The ones with $z_\lambda(\mathbf{k})=0$ at $k=0$ are called hydrodynamic modes, all the rest are called kinetic modes. Next we consider the eigenvectors. In (1.50) we have already determined the zero eigenvectors $q_\lambda(\mathbf{c})$ of $\Omega^{(1)}$ which represent the right eigenvectors Ψ_λ in the long wavelength limit $(\mathbf{k}\to 0)$. Denoting the eigenvectors as

$$\mid q_\lambda\rangle_i = \{\mid\rho\rangle_i, \mid\mathbf{g}\rangle_i, \mid\epsilon\rangle_i\} = k_i\{1,\mathbf{c}_i,\frac{1}{2}c_i^2\} \tag{1.57}$$

the eigenvalue equations (1.50) and (1.9) can be written as

$$\Omega^{(1)}\mid q_\lambda\rangle = 0, \qquad \langle q_\lambda\mid\Omega^{(1)} = 0 \tag{1.58}$$

The left eigenvectors, $\langle\phi_\lambda\mid$, defined through the relation,

$$\langle\phi_\lambda(\mathbf{k})\mid e^{-i\mathbf{k}\cdot\mathbf{c}}(\mathbf{1}+\Omega^{(1)}) = e^{z_\lambda(\mathbf{k})}\langle\phi_\lambda(\mathbf{k})\mid \tag{1.59}$$

differ from the right eigenvectors $\mid \Psi_\lambda(\mathbf{k})\rangle$. By taking the transpose of (1.59), using the symmetry of thermal inner product (1.46) discussed in references [12,20], and comparing it with (1.55) we deduce,

$$\phi_\lambda(\mathbf{k}) = e^{-i\mathbf{k}\cdot\mathbf{c}}\Psi_\lambda(\mathbf{k})/M_\lambda \tag{1.60}$$

where M_λ is a normalization constant. The right or the left eigenvectors are not orthogonal, but form a complete biorthonormal set, satisfying,

$$\sum_\lambda \mid \Psi_\lambda\rangle\langle\phi_\lambda \mid = \mathbf{1} \tag{1.61}$$

$$\langle\phi_m \mid \Psi_\lambda\rangle = \langle\psi_m \mid e^{-i\mathbf{k}\cdot\mathbf{c}} \mid \Psi_\lambda\rangle/M_\lambda = \delta_{m\lambda}$$

With the help of these eigenfunctions we make the following spectral decomposition of the Boltzmann propagator (1.53),

$$\Gamma(\mathbf{k},t)k = \sum_\lambda \mid \Psi_\lambda(\mathbf{k})\rangle e^{z_\lambda(\mathbf{k})}\langle\phi_\lambda(\mathbf{k}) \mid \tag{1.62}$$

With the above notations the structure factor (1.54) can be written as

$$\rho S(\mathbf{k},\omega) = 2Re\langle\rho \mid [e^{i\omega+\mathbf{k}\cdot\mathbf{c}} - 1 - \Omega^{(1)}]^{-1} + \frac{1}{2} \mid \rho\rangle \tag{1.63}$$

$$= 2Re\sum_\lambda \langle\rho \mid \Psi_\lambda\rangle\langle\phi_\lambda \mid \rho\rangle\{e^{i\omega - z_\lambda(\mathbf{k})} - 1 + \frac{1}{2}\}$$

$$= 2Re\sum_\lambda N_\lambda \left\{\frac{1}{e^{i\omega - z_\lambda(\mathbf{k})} - 1} + \frac{1}{2}\right\}$$

$$= 2Re\sum_\lambda N_\lambda[i\omega - z_\lambda(\mathbf{k})]^{-1}[1 + O(k^2)] \tag{1.64}$$

where we used the relation $(e^x - 1)^{-1} + \frac{1}{2} \simeq x^{-1}$ valid for small x.

In order to obtain expressions for the N_λ and the $z_\lambda(\mathbf{k})$ we expand the hydrodynamic modes $\Psi_\lambda(\mathbf{k})$ and eigenvalues $z_\lambda(\mathbf{k})$ in a Taylor-series with ik as a small parameter

$$\Psi_\lambda(k) = \Psi_\lambda^{(0)} + ik\Psi_\lambda^{(1)} + (ik)^2\Psi_\lambda^{(2)} \tag{1.65}$$

$$z_\lambda(\mathbf{k}) = ikz_\lambda^{(0)} + (ik)^2 z_\lambda^{(2)} \tag{1.66}$$

We refer to [21] for detailed analysis of this expansions in terms of the eigenfunctions (1.58) for $\mathbf{k} = 0$. The coefficients of the expansion can be expresses in terms of

thermodynamic derivatives such as the speed of sound c_s, and transport coefficients (see also Sec.1.9) such as the kinematic viscosity ν, the heat diffusivity D_T, and the sound damping constant Γ. It is shown that the dominant contributions to the structure factor in small k approximation come from hydrodynamics modes: the shear mode ($\lambda = \perp$), the heat mode ($\lambda = T$) and the two sound modes ($\lambda = \sigma = \pm$). In particular, the expansion (1.66) reduces to

$$\begin{aligned} z_\perp(k) &= -\nu k^2 \\ z_T(k) &= -D_T k^2 \\ z_\sigma(k) &= -i\sigma c_s k - \Gamma k^2 \end{aligned} \tag{1.67}$$

and the coefficients N_λ as defined in (1.64) are found to be

$$N_\sigma = \frac{\langle \delta\rho^2 \rangle}{2\gamma}\left\{1 + \frac{ik}{\sigma c_s}[\Gamma + (\gamma - 1)D_T]\right\} + O(k^2) \tag{1.68}$$

$$N_T = \langle \delta\rho^2 \rangle \left(\frac{\gamma - 1}{\gamma}\right) + O(k^2)$$

$$\gamma = \frac{\langle \delta p^2 \rangle \langle \delta\rho^2 \rangle}{\langle \delta p \delta\rho \rangle^2}$$

$$N_\perp = 0$$

The sound damping constant Γ is found to be dependent on the other coefficients as:

$$\Gamma = \frac{1}{2}\nu + \frac{1}{2}(\gamma - 1)D_T \tag{1.69}$$

Finally, the combination of (1.64), (1.69) yields the expression for dynamic structure factor in the hydrodynamic regime, known in the literature as the Landau-Placzek approximation:

$$\begin{aligned} \frac{S(\mathbf{k},\omega)}{S(\mathbf{k})} &= \left(\frac{\nu - 1}{\nu}\right)\frac{2D_T k^2}{\omega^2 + (D_T k^2)^2} + \frac{1}{\nu}\sum_{\pm}\frac{\Gamma k^2}{(\omega \pm c_s k)^2 + (\Gamma k^2)^2} \\ &+ \frac{1}{\nu}[\Gamma + (\nu - 1)D_T]\frac{k}{c_s}\sum_{\pm}\frac{(c_s k \pm \omega)}{(\omega \pm c_s k)^2 + (\Gamma k^2)^2} \end{aligned} \tag{1.70}$$

The first two terms in (1.70) represent three symmetric Lorentzians. The first one is the Rayleigh peak with a width $D_T k^2$ and the other two Doppler shifted ($\pm c_s k$)

lines are the Brillouin peaks with a width Γk^2. The last term in (1.70) describes asymmetric contributions to the Brillouin lines (there are no asymmetric corrections to the Rayleigh line).

The power spectrum (1.70) consisting of the Rayleigh line and the asymmetric Brillouin lines, derived here from the Boltzmann equation for the lattice gas, is completely analogous to the results of the Landau-Placzek theory for continuous isotropic fluids [22].

1.9 Transport coefficients

The hydrodynamic equations for the macroscopic local densities $q(\mathbf{r},t) = \{\rho(\mathbf{r},t), \mathbf{g}(\mathbf{r},t), \varepsilon(\mathbf{r},t), q_s(\mathbf{r},t)\}$ (see for example Eqs. (1.6)-(1.8)) are obtained [6] by averaging the microscopic local conservation laws (1.10) and by making leading order expansion in the gradients of the thermodynamics fields around equilibrium. The coefficients in this expansion are the thermodynamic succeptibilities (*e.g.*, sound velocity) and the transport coefficients $L_{qq'}$ which define the linear response of a system to an external perturbation [23]

$$J_q(\mathbf{r},t) = -\sum_{q'} L_{qq'} \nabla b_{q'}(\mathbf{r},t) \tag{1.71}$$

where $\{\nabla b_{q'}\}$ is the set of thermodynamic driving forces. $J_q(\mathbf{r},t)$ is the longitudinal current associated with the conserved density $q(c_i) = \{1, \mathbf{c}_i, \frac{1}{2}c_i^2, ...\}$

$$J_q(\mathbf{r},t) = \sum_i c_{ix} q(c_i) \delta n_i(\mathbf{r},t) \tag{1.72}$$

The currents $J_q(\mathbf{r},t)$ associated with the different conserved densities $q(c_i)$ are required to be distinct. Thus it is conventional [4] to define *subtracted* currents

$$\hat{J}_q = J_q - \delta Q \langle \delta Q \delta Q \rangle^{-1} \langle \delta Q J_q \rangle = \sum_{\mathbf{r}i} \hat{j}_q(c_i) \delta n(\mathbf{r},t) \tag{1.73}$$

which are mutually orthogonal in terms of the thermal product (1.46). Here $\{Q\}$ are the global invariants as defined in (1.11). The single-particle currents $\hat{j}_q(c_i)$ will be specified when discussing specific transport coefficients for specific models (see Section 2.2 for example).

To compute the $L_{qq'}$ we use the well-known Green-Kubo formulas for continuous fluids [4,23] with a few minor adaptations for the discreteness of space and time. Thus the transport coefficient $L_{qq'}$ for any d-dimensional thermal LGCA is given [24] by

$$L_{qq'} = \lim_{s \to 0} V^{-1} \sum_{t=0}^{\infty *} e^{-st} \langle \hat{J}_q(t) \hat{J}_{q'} \rangle \tag{1.74}$$

where V is the total number of sites in the system. The two minor modification of the Green-Kubo formulas for continuous fluids are: the appearance of an asterisk

and of a discrete time sum instead of an integral. The asterisk on the summation indicates that the term with $t = 0$ has a weight $\frac{1}{2}$. Green-Kubo relations contain subtracted currents as defined in (1.73). The transport matrix $L_{qq'}$ for LGCA fluids is a nonnegative matrix, implying that $L_{qq} \geq 0$ for all q. It may also include the spurious transport coefficients, connected with the spurious modes (if any are present).

Next we discuss the specific transport coefficients that appear in the fluid dynamic equations. The *heat conductivity* λ (the thermal diffusion coefficient D_T) is defined as the coefficient of proportionality between the dissipative heat current and the temperature (reciprocal temperature) gradient, *i.e.*,

$$\mathbf{q}^D = -\lambda \nabla T \equiv L_{TT} \nabla \beta \qquad with \qquad L_{TT} = D_T = k_B T^2 \lambda \tag{1.75}$$

Similarly to the theory of continuous fluids, we switch to the tensor description of transport phenomena related to the gradient of the vector flow field $\mathbf{u}$, introducing the fourth-rank viscosity tensor for the LGCA, which relates the dissipative part of the stress tensor to the gradient of the flow field

$$\sigma^D_{\alpha\beta} = -\rho \nu_{\alpha\beta\gamma\delta} \nabla_\gamma u_\delta \tag{1.76}$$

where $\alpha\beta\gamma\delta = \{x, y, z, ...\}$ label Cartesian components. We restrict ourselves to those models which provide a fourth-rank tensor $\nu_{\alpha\beta\gamma\delta}$ having the full fluid symmetry so that it can be expressed in terms of two independent scalars. We then obtain the shear viscosity $\nu = \nu_{\alpha\beta\alpha\beta}$ and the bulk viscosity $\zeta = (\frac{1}{d^2})\nu_{\alpha\alpha\beta\beta}$ in the well known form from continuous fluid theory

$$\nu_{\alpha\beta\gamma\delta} = \nu(\delta_{\alpha\gamma}\delta_{\beta\delta} + \delta_{\alpha\delta}\delta_{\beta\gamma} - \frac{2}{d}\delta_{\alpha\beta}\delta_{\gamma\delta}) + \zeta \delta_{\alpha\beta}\delta_{\gamma\delta} \tag{1.77}$$

The Green-Kubo relations (1.74) considered so far are exact. They require the solution of the complete N-body dynamics (1.2). But we can readily obtain the *Boltzmann approximation* to any transport coefficient in terms of the eigenfunctions Ψ_λ and eigenvalues α_λ of the linearized Boltzmann collision operator $\Omega^{(1)}$ defined in (1.44). Closely following the analysis given in Refs.[9,12], we find that the Green

Chapter 2

FHP-1 Lattice Gas Model

In this chapter we will illustrate the predictions of LGCA theory for the simplest lattice gas models which have the features necessary to yield, in the appropriate approximation, the standard Navier-Stokes equations for continuum fluids. That is, we will not consider models with spurious conservation laws or with insufficient isotropy of the underlying lattice. In the set of conserved quantities we include only the particle number and momentum. The simplest way to achieve this is to consider models with all particles having the same speed. The energy, therefore, just corresponds to the number of particles and is not an independent conserved scalar. The general theoretical results for LGCA given in Chapter 1 are easily adapted to such models, referred to in the literature [13,18] as *athermal* models, by disregarding all the terms which relate to the energy as a conserved quantity. Most of this Chapter deals with a simple example of such an athermal model: the 6-bit FHP-1 model.

2.1 Introduction to FHP-class models

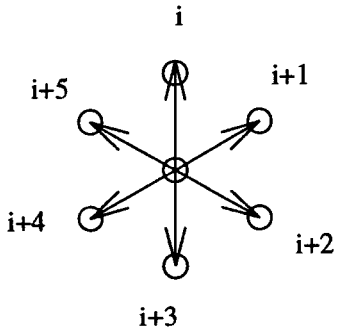

Figure 2.1: Enumeration of possible states (or velocity channels) in the FHP-1 model

The FHP models, introduced by Frish, Hasslacher and Pomeau [1,6], are very simple. The underlying lattice is triangular with unit lattice constant. Each node is connected to its six neighbors by units vectors $\mathbf{c}_i$ [1] (with i defined modulo six) [2] (see Figure 2.1) and is thus endowed with six-bits. As discussed earlier in Section 1.3, updating involves propagation and collisions.

Possible collision processes are shown in Figure 2.2. When constructing collision rules for these processes we must consider both *deterministic* and *nondeterministic* rules as defined in Section 1.6. For a head-on collision with occupied "input channels" $(i, i+3)$ shown in Fig.2.2(a), there are two possible pairs of occupied "output channels" such that mass and momentum are conserved, namely $(i+1, i+4)$ shown in Fig.2.2(b) and $(i-1, i-4)$ shown in Fig.2.2(c). We can decide always to choose one of these channels; we then

[1] these are the lattice vectors

[2] meaning that the summation operation on indices has the cyclic property: 6+1 = 1, 6+2 = 2, 5+2 = 1, etc

have a deterministic model, which is *chiral*. i.e., not invariant under mirror-symmetry. Alternatively, we can make a nondeterministic (random) choice, with equal probabilities to restore mirror-symmetry. Finally, we can make a pseudo-random choice, dependent, for example, on the parity of a time or space index.

We must also ensure the absence of *spurious conservation laws*. For example *if* we consider the model which include head-on collisions *only* then we have a model with one extra globally conserved quantity. This is because the head-on collisions conserve, in addition to total particle number, the difference of particle numbers in any pair of opposite directions $i, i+3$, namely $\sum_{\mathbf{r}}(n_i(\mathbf{r},t) - n_{i+3}(\mathbf{r},t))$. This means that in addition to mass and momentum conservation, there is a spurious conservation law. The large-scale dynamics of such a model will differ drastically from ordinary hydrodynamics, unless the spurious conservation law is removed [6]. One way to achieve this is to introduce triple collisions $(i, i+2, i+4) \rightarrow (i+1, i+3, i+5)$ (see Fig.2.2(d)(e)). Then each time the triple collision occurs, the difference of particle numbers along each of the three lattice directions changes.

Several models can be constructed on the triangular lattice. The simplest set of collision rules with no spurious law, called the FHP-1 model, involves (random) binary head-on collisions and triple collisions. This is the model that we analyze in detail below.

The model FHP-2 is a seven-bit variant of FHP-1 including a zero-velocity *rest particle*, and variants of the head-on and triple collisions with a *spectator* rest particle. A spectator particle is one which is available at the site during a collision but which does not take part in the scattering process. It was shown [6] that binary collisions involving rest particles remove the spurious conservation laws, and do so more efficiently at low densities than triple collisions. The set of collision rules can be saturated by inclusion of the duals of the head-on collisions and head-on collisions with a spectator. In this way we arrive at the FHP-3 model which is a collision-saturated version of FHP-2 [6].

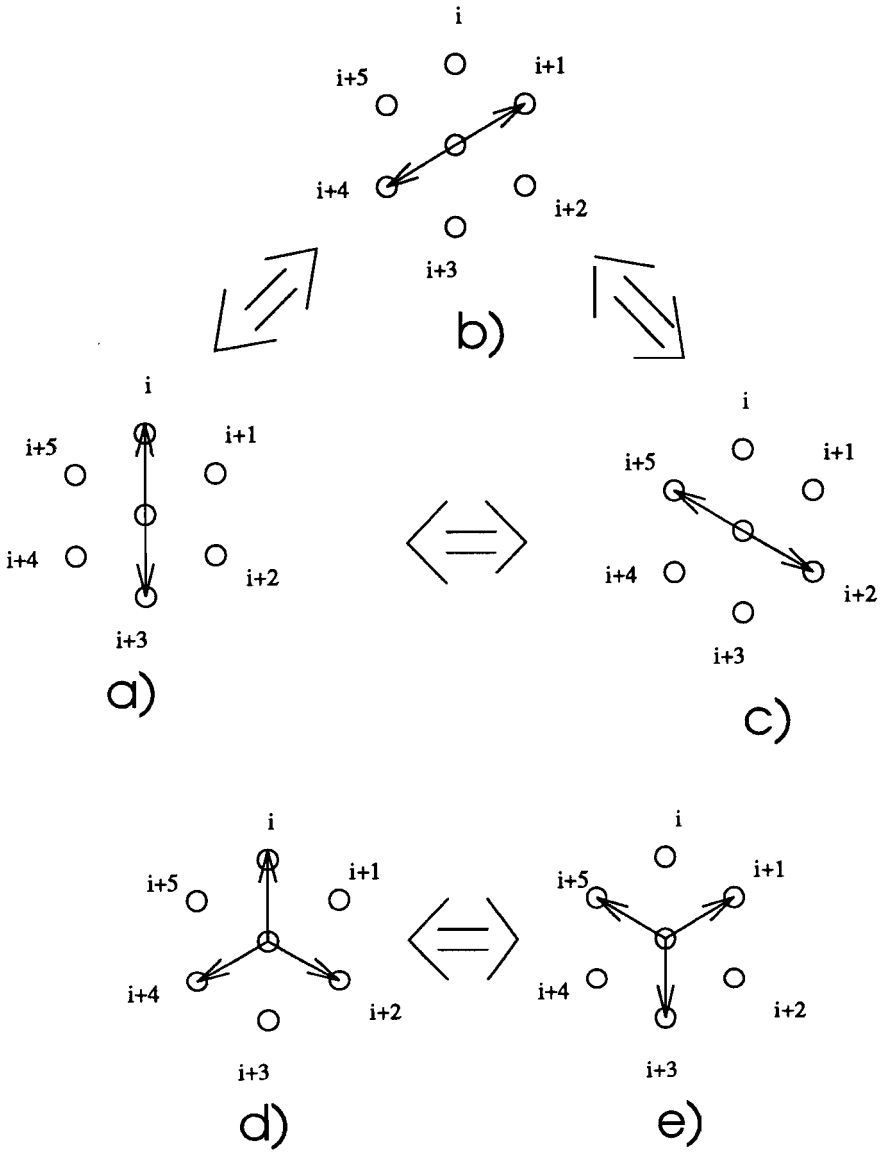

Figure 2.2: Collision rules for the FHP-1 model with $a), b), c)$ head-on collision with two equiprobable outcomes and $d), e)$ triple collision.

An interesting question arrises when we consider the FHP model with rest particles. The availability of different particle speeds (and hence the different energy levels) allows us to define the thermodynamic temperature of the system. However, the FHP-2 and FHP-3 models do not belong to the category of thermal models. Indeed, FHP models with rest particles do not have interesting thermal properties. Their coefficient of thermal diffusion (1.75) is found to be equal to zero, because of the zero-value of the corresponding subtracted current (1.73) (See Eq.(2.14) and discussion afterwards). Physically this can be explained because the zero-velocity particles do not participate in any kind of diffusion, so that the thermal diffusion coefficient is the same as that of the one-speed models.

2.2 Collision Matrix

To analyze the lattice Boltzmann equation (1.15) for the FHP-1 model we need to have the explicit form for the Collision operator introduced in (1.2). To obtain this, we enumerate all possible states (velocity channels) at one site according to the diagram displayed in Fig. 2.1 As discussed in Section 1.3 of the first chapter, each term of the collision operator is constructed from the change in the number of type "i" particles due to a particular type of collision, multiplied by the probability of the arrangement of particles involved in that collision. In the Boltzmann approximation this probability is a simple product of the densities f_i for particles that should be present, multiplied by factors $(1 - f_j)$ for particles that should be absent.

Then the probabilities of states $(a), (b), (c)$ as shown in Fig. 2.2 are written as:

$$\begin{aligned} (a) \quad & f_1 f_4 (1-f_2)(1-f_3)(1-f_5)(1-f_6) = P_{14} \\ (b) \quad & f_2 f_5 (1-f_1)(1-f_3)(1-f_4)(1-f_6) = P_{25} \\ (c) \quad & f_3 f_6 (1-f_1)(1-f_2)(1-f_4)(1-f_5) = P_{36} \end{aligned} \tag{2.1}$$

In general the state with $i_1, i_2, ..., i_k$ particles present has the following probability:

$$P_{i_1,i_2,...,i_k} = \frac{f_{i_1}}{1-f_{i_1}} \frac{f_{i_2}}{1-f_{i_2}} ... \frac{f_{i_k}}{1-f_{i_k}} \prod_{i=1}^{6} (1-f_i) \tag{2.2}$$

Hence the collision rules displayed in Fig. 2.2 contribute the following terms to the collision matrix:

$$\begin{aligned} \Omega_1 = & -P_{14} + \frac{1}{2} P_{25} + \frac{1}{2} P_{36} \\ & - P_{135} + P_{246} \end{aligned} \tag{2.3}$$

with P_{135} and P_{246} being the probabilities of state (d) and (e) of Fig. 2.2 respectively. The other $\Omega_i (i = 1, 6)$ are given by a cyclic shift of the indices, as a result of the hexagonal symmetry of the lattice.

Rather tedious algebra has to be done to get the linearized Boltzmann collision matrix as defined by (1.38)-(1.39). The expansion (1.39), for example, gives the

following expression for the P_{14} term in (2.1)

$$P_{14} = f\bar{f}^4 + f\bar{f}^3(\bar{f}, -f, -f, \bar{f}, \bar{f}, -f, -f) \otimes \Phi \tag{2.4}$$

with Φ being the column vector with six elements $\Phi_i, i = \{1, 2, ..., 6\}$. Here $f = f_i^0$ is the equilibrium solution which does not depend on the index i for the FHP-1 model and $\bar{f} = 1 - f$.

A similar procedure applied to the other terms in the collision operator gives the following expression for the first row of the linearized collision matrix

$$\Omega_{1i}^{(1)} = f\bar{f}^2[-1, \frac{1}{2}(1+f), \frac{1}{2}(1-3f), 2f-1, \frac{1}{2}(1-3f), \frac{1}{2}(1+f)] \tag{2.5}$$

Because in the FHP-1 model all particle types are equivalent up to a lattice symmetry transformation, other rows of the $\Omega^{(1)}$ matrix are given simply by cyclic shifts the first row so that the complete form of $\Omega^{(1)}$ is determined from the first row (2.5). $\Omega^{(1)}$ can therefore, be written as a circulant matrix

$$\Omega^{(1)} = f\bar{f}^2 circ[-1, \frac{1}{2}(1+f), \frac{1}{2}(1-3f), 2f-1, \frac{1}{2}(1-3f), \frac{1}{2}(1+f)] \tag{2.6}$$

(In terms of the probabilities γ for different types of collisions, we can obtain the expression (2.6) from the general result (4.4.7) of Ref.[18], using $\gamma_2 = 1$, $\gamma_{2L} = \frac{1}{2}$, $\gamma_{3s} = 1$, $\gamma_{3A} = \gamma_{4*} = 0$).

With this explicit form of the linearized collision matrix we are now ready to approach the eigenvalue problem (1.55). In general this problem cannot be solved analytically although for $\mathbf{k} = 0$ it reduces to Eq.(1.44), and for the FHP-1 model can be trivially solved because of the circulant property of the collision matrix [25]. In this case the result for the eigenvectors of (2.6) reads [18]:

$$\begin{aligned} v_1 &= \frac{1}{\sqrt{6}}(1,1,1,1,1,1) \\ v_2 &= \frac{1}{\sqrt{6}}(1,\sigma,-\sigma^*,-1,-\sigma,\sigma^*) = (v_6)^* \\ v_3 &= \frac{1}{\sqrt{6}}(1,-\sigma^*,-\sigma,1,-\sigma^*,-\sigma) = (v_5)^* \\ v_4 &= \frac{1}{\sqrt{6}}(1,-1,1,-1,1,-1) \end{aligned} \tag{2.7}$$

where

$$\sigma = exp(i\pi/3) = \frac{1}{2}(1 + i\sqrt{3}) \tag{2.8}$$

and the corresponding eigenvalues are

$$\begin{aligned} \lambda_1 &= 0 \\ \lambda_2 &= 0 \\ \lambda_3 &= -3f^1\bar{f}^3 \\ \lambda_4 &= -6f^2\bar{f}^2 \\ \lambda_5 &= (\lambda_3)^* \\ \lambda_6 &= 0 \end{aligned} \tag{2.9}$$

As it is expected from theory (see Sec.1.7) the matrix $\Omega^{(1)}$ has three zero eigenvalues corresponding to the hydrodynamic modes, i.e. the corresponding eigenvalues are associated with the conserved quantities of the system [18]. In the next sections we will show that analytical continuation to $k \neq 0$ shows all the behavior of the hydrodynamic modes of real fluids within a small range $k \leq k_h$ which thus justifies the FHP-1 model as a valid representation for linear hydrodynamics.

2.2.1 FHP transport coefficients in Boltzmann approximation

We can now evaluate the transport coefficients of the FHP-1 model in Boltzmann approximation. It will be useful also to comment on the values for other FHP models.

For the FHP-1 model the combination of (1.81) (1.84) and (1.77) with the explicit form of the Boltzmann collision matrix (2.6) gives

$$\nu = \frac{1}{12}\frac{1}{f(1-f)^3} - \frac{1}{8} \tag{2.10}$$

$$\zeta = 0 \tag{2.11}$$

where $f = \frac{\rho}{6}$ is the mean density per channel. The result for the shear viscosity (2.10) will be discussed and compared with results of computer simulations of the FHP-1

model in the next sections. The zero value of the bulk viscosity ζ results from the observation that the diagonal terms of the respective subtracted current (1.84) are identically equal to zero. However we have non-zero bulk viscosity for other FHP models with rest particles.

The thermal diffusion coefficient D_T is identically zero for all FHP models, even those for which a temperature can be defined (see Sec.2.1). This comes about because the corresponding subtracted current $\hat{j}_e$ is equal to zero:

$$j_e = \sum_{\mathbf{ri}} c_{ix} \frac{1}{2} c_i^2 \delta n_i(\mathbf{r}, t) \tag{2.12}$$

$$\hat{j}_e = j_e - \delta\varepsilon \frac{\langle \delta\varepsilon j_e \rangle}{\langle \delta\varepsilon \delta\varepsilon \rangle} \tag{2.13}$$

$$= \sum_{\mathbf{ri}} \left(\frac{1}{2} c_i^2 c_{ix} - \frac{1}{2} \frac{\sum_j c_{jx} \frac{1}{4} c_j^4 k_j}{\sum_j \frac{1}{4} c_j^2 k_j} \right) \delta n_i(\mathbf{r}, t) = 0 \tag{2.14}$$

We used the expression for the density fluctuation correlation (1.36) to obtain the left-hand-side of (2.14).

For the FHP-1 model this expression vanishes because the speed $\mid c_i \mid$ is the same for each velocity channel i, and thus can be taken outside the summation as a constant. For FHP models with rest particles, the same result hold true because the rest particles do not contribute to any of the terms. Thus we have

$$D_T = 0 \tag{2.15}$$

for all FHP models.

2.3 Structure of spectra

We now study the hydrodynamic dispersion relations $z_\lambda(\mathbf{k})$ (1.55) of spatial fluctuations in the occupation of single-particle states, which provide basic information about the collective excitations and their relevant time and length scales as discussed in Section 1.8. The spectra show how the speed of sound, damping constants, and transport coefficients depend on the wavelength of the excitations, on the thermodynamic variables, and on the microscopic details of the models. In this manner

we are able to develop important and practical criteria to judge the applicability of lattice-gas models for the study of flow properties.

The set of (real parts of) the eigenvalues $z_\lambda(\mathbf{k})$ determines the basic set of relaxation constants or time scales in the problem. Given the frequency or wavelength of interest one can judge from the spectrum which eigenmodes of the kinetic equation are relevant. Similarly to the theory of continuous fluids the range of wavelength and time scales of interest is compared to the mean free path l_0 and the mean free time t_0 respectively. As a result we distinguish three different regimes:

- a *hydrodynamic regime* (HR). Here $kl_0 \ll 1$. This is the regime most relevant for scattering experiments on fluids, where the Landau-Placzek theory (Sec.1.8) fully explains the dynamic scattering function $S(\mathbf{k},\omega)$ in terms of the slow hydrodynamic modes (1.67). It is the main focus of our interest.

- a *regime of generalized hydrodynamics* (RGH). The hydrodynamic modes are still dominant here, but unlike in the hydrodynamic regime, the speed of sound and transport coefficients (viscosities, etc.) become k dependent. The typical wavelengths and time scales are of the order of the mean free path ($kl_0 \simeq 1$). This case is analogous to the kinetic regime in the theory of continuous fluids and is typical for gases under normal pressure and temperatures [22].

- Finally when the wavelengths are small compared to l_0 we have a *lattice regime* which is analogous to the free particle (or Knudsen) regime ($kl_0 \gg 1$) in the kinetic theory of gases.

To estimate the mean free path l_0 for the FHP-1 model in terms of density ρ or channel density f, we recall that the physical meaning of the collision matrix is the change of particle population in unit time. So we can introduce a relevant time scale t_0 by

$$\Omega \simeq \frac{1}{t_0}\mathbf{1} \tag{2.16}$$

and interpret it as the mean time during which one scattering process takes place.

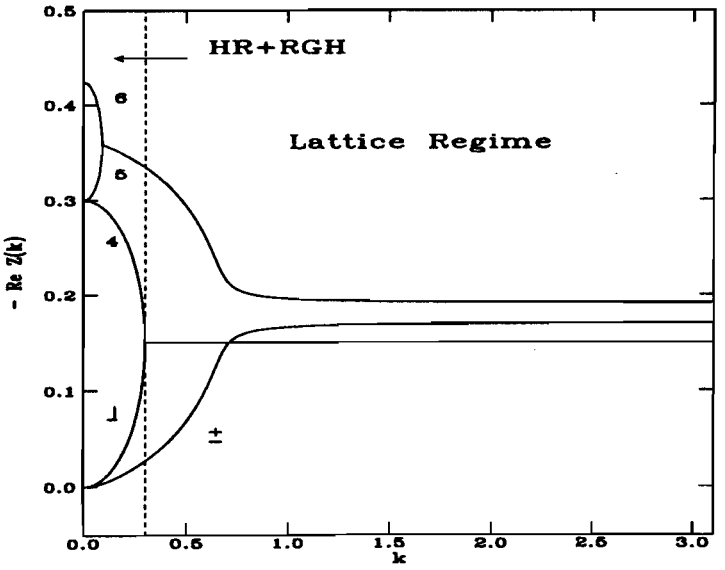

Figure 2.3: Real part of the spectrum $z_\lambda(\mathbf{k})$, for the six-bit FHP-1 model at $\rho = 2.4$, vs k for $\mathbf{k} \parallel \hat{x}$. HR+RGH stands for *Hydrodynamics Regime + Regime of Generalized Hydrodynamics* and corresponds to the region $k < k_1 = 0.3$ indicated by the dashed line

Comparing (2.16) and (2.6) we evaluate the mean free path l_0 as

$$l_0 = \mid c_i \mid t_0 \simeq \frac{1}{f(1-f)^2} \tag{2.17}$$

Next we consider the solutions of equation (1.55) as a function of k-vector and study the spectrum in different regimes. The complexity of the collision matrix makes most of the spectrum accessible only by numerical methods. Analytical results can be obtained by perturbative methods when the wavelength is large or small compared to the mean free path, as was illustrated in Section 1.8.

This section describes the numerical study of the FHP-1 model spectra. The numerical problem is rather simple. It involves the calculation of the six roots of the secular determinant of the complex matrix in (1.55) as a function of the reciprocal lattice vector $\mathbf{k}$. The eigenvalues $z_\lambda(\mathbf{k}) = Rez_\lambda(\mathbf{k}) + iImz_\lambda(\mathbf{k})$ are in general complex and the resulting dispersion relation of model with density $\rho = 2.4$ are shown in Figures 2.3 (real part) and 2.4 (imaginary). All six eigenvalues are plotted against $\mathbf{k}$ directed along the $\hat{x}$ axis in reciprocal space.

The spectrum of Figures 2.3 and 2.4 shows three soft hydrodynamics modes,

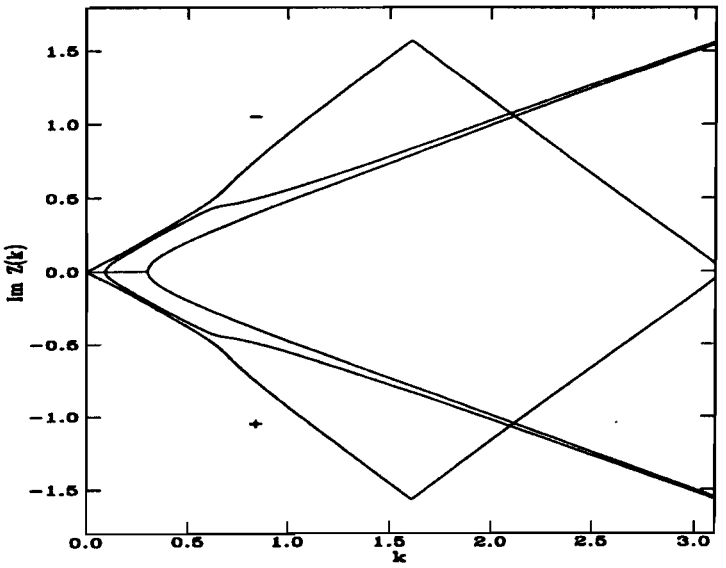

Figure 2.4: Imaginary part of the spectrum $z_\lambda(\mathbf{k})$, for the six-bit FHP-1 model at $\rho = 2.4$, vs k for $\mathbf{k} \parallel \hat{x}$

labeled $\perp \pm$ and three hard kinetic modes with $Rez_\lambda(0) < 0$, labeled 4,5,6.

The $k = 0$ values of the spectrum are related to the eigenvalues of the linearized collision matrix (2.9) by Eq.(1.56). For $f = \rho/6 = 0.4$ the values of the kinetic modes are $z_4(0) = 0.3011, z_5(0) = z_6(0) = 0.4311$. This agrees with the $\mathbf{k} = 0$ result of Fig. 2.3.

The hydrodynamic modes consist of two propagating damped sound modes ($\lambda = \pm$) with $Imz_\pm(\mathbf{k}) = \mp c(\mathbf{k})k$ and one diffusive shear mode ($\lambda = \perp$) with $Imz_\perp(\mathbf{k}) = 0$. The real parts of $z_\pm(\mathbf{k})$ coincide. All the real parts of the hydrodynamic modes equal zero at ($\mathbf{k} = 0$) in accordance with (2.9) and the discussion afterwards. The real parts of the hydrodynamic and kinetic eigenvalues are well separated for $k < k_1$, where k_1 is the wave number at which for the first time a hydrodynamic and kinetic eigenvalue are equal. Wave numbers rather smaller than k_1 characterize the regime of generalized hydrodynamics (RGH). In our case we have $k_1 \simeq 0.3$ at $\rho = 2.4$. It is interesting to note that the mean free path as calculated from (2.17) is approximately 7 lattice units. This allows us to estimate the kinetic regime as $k \simeq k_1' = \frac{1}{l_0} = 0.15$ which is indeed of the same order as k_1.

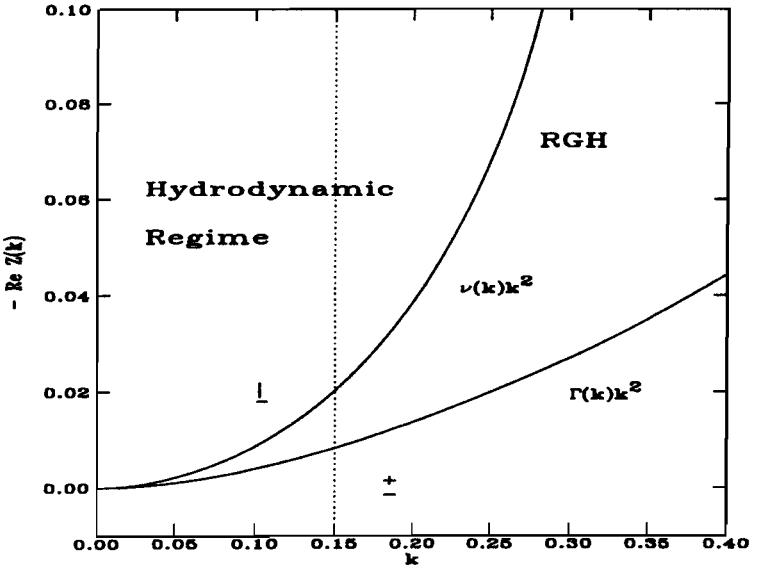

Figure 2.5:
Small k region of the spectrum of Fig.2.3. In the hydrodynamic regime $k < k_h = 0.15$ (k_h is indicated by the dotted line) $\nu(k)$ and $\Gamma(k)$ do not depend on k, while in the regime of generalized hydrodynamics they do.

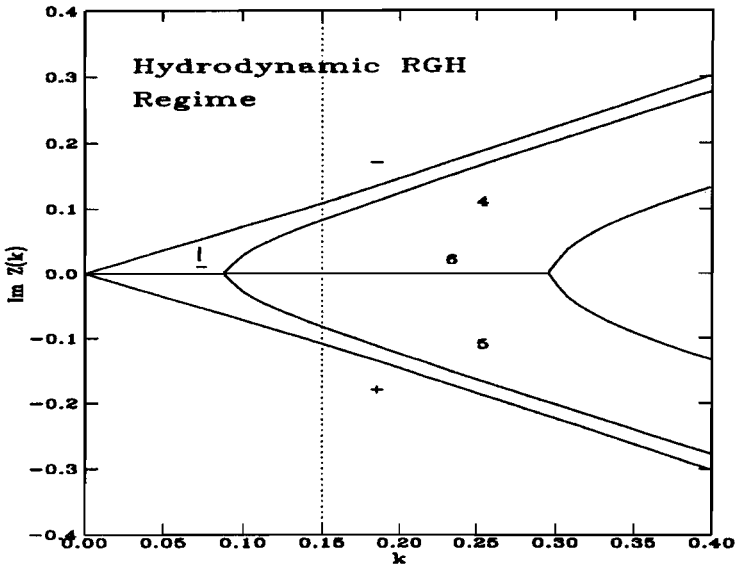

Figure 2.6: Small k region of the spectrum of Fig.2.4.

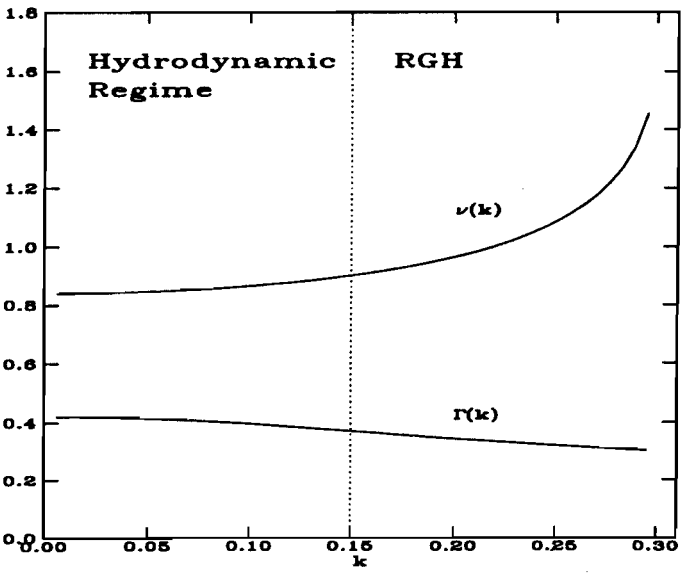

Figure 2.7:
Diffusive shear mode divided by k^2 and sound mode (real part) divided by k^2 plotted against k. The value of k beyond which these functions are no longer constant is $k_h \simeq 1.5$. This is the upper bound of the hydrodynamic regime. The shear viscosity ν and sound damping constant Γ defined in (1.67) are evaluated as 0.85 and .42 respectively.

In the limit of small k ($k \ll k_1$) the eigenvalues are given by the hydrodynamic dispersion relations (1.67). From Fig.2.7 we estimate the maximum value of the k-vector k_h where those relations are still valid. Within a tolerance of 5%, the shear viscosity and the sound damping constant, as calculated from data of Fig.2.5, do not depend on k in the region of $k < k_h \simeq 0.15$ and are equal to 0.85 and 0.42 respectively. This is in good agreement with the values $\nu = 0.84$ and $\Gamma = 0.42$ calculated using Eqs.(2.10) and (1.69). A similar geometrical analysis of Fig.2.8 gives the value of sound velocity as $c_s = 0.73 \simeq \frac{1}{\sqrt{2}} = 0.707$ (see Sec.1.6).

Finally, we mention some important features of the spectrum beyond the hydrodynamic regime and their relation to the parameters and coefficients defined for the hydrodynamic regime.

When k increases, the dispersion relations of classical hydrodynamics with k-independent transport coefficients break down and we enter the regime of generalized hydrodynamics, where the dispersion relations can be represented approximately by

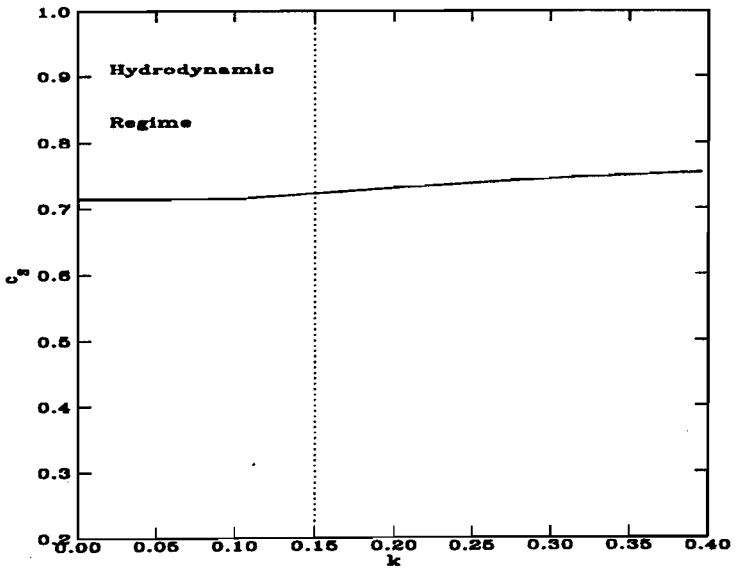

Figure 2.8:
Sound mode (imaginary part) over k plotted against k. The $k \to 0$ limit of the plot corresponds to the speed of sound and equals 0.73.

(1.67) with a slowly varying $\mathbf{k}$ dependent speed of sound $c_s(\mathbf{k})$ and $\mathbf{k}$-dependent transport coefficients $\Gamma(\mathbf{k})$ and $\nu(\mathbf{k})$ (see Fig.2.7). This regime was recently analysed by Das and co-workers [26]. They showed that the $\mathbf{k}$ dependence of transport coefficients explains some older simulation results obtained for six-bit FHP lattice gases with a small number of allowed collisions. In particular they resolved the puzzling observations of a negative bulk viscosity in References [2] and [27].

Upon further increase of the wave vector we enter the lattice regime ($k > k_1$, where k_1 is indicated by the dashed line in Figures 2.3, 2.9, 2.10) where the excitation wavelength is smaller than the mean free path of the particles. This regime does not provide any significant physical information about the model. As mentioned earlier, the lattice regime is similar to the free particle regime in the low density limit and hence can be described by means of perturbation theory. In first order the spectrum $z_\lambda(\mathbf{k})$ can be written [26] as:

$$z_\lambda(\mathbf{k}) = -i\mathbf{k}\cdot\mathbf{c}_i + \Omega_{ii}^{(1)} \simeq -i\mathbf{k}\cdot\mathbf{c}_i - f(1-f)^2 \qquad (2.18)$$

therefore $-Rez_\lambda(\mathbf{k}) = f(1-f)^2$ is expected to be six-fold degenerate. This is not

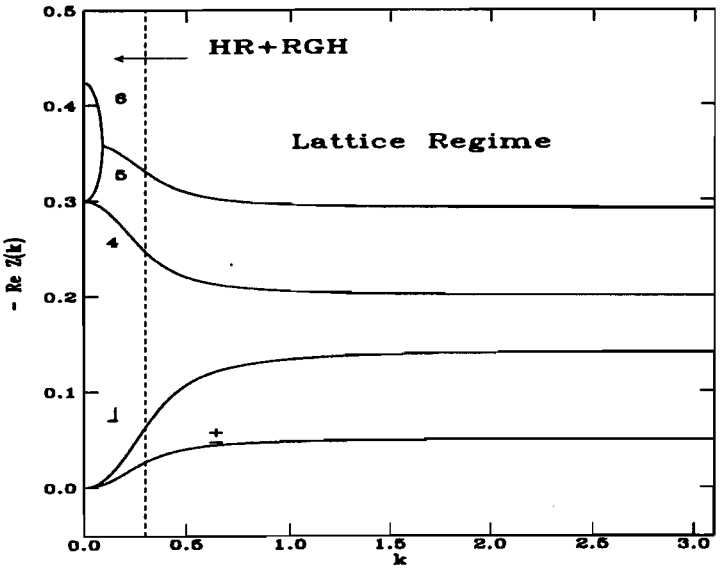

Figure 2.9:
Real part of the spectrum $z_\lambda(\mathbf{k})$, for the six-bit FHP-1 model at $\rho = 2.4$, vs k for $\mathbf{k} \parallel \hat{y}$.

exactly the case for density $\rho = 2.4$, as we see in Fig.2.3, however all the modes in the lattice regime differ only slightly one from another and from the value $\Omega_{ii}^{(1)} = 0.14$ obtained from Eq.(2.18).

Finally we study the effects of the direction of the vector $\mathbf{k}$ and of the lattice gas density on the crossovers between the three defined LGCA regimes. Figure 2.9 shows the spectrum with same parameters as in Fig.2.3, but with $\mathbf{k}$ parallel to $\hat{y}$. We observe that the spectrum is approximately independent of the direction of $\mathbf{k}$ for small k within the hydrodynamic regime. For $k > k_1 = 0.3$ (shown as the dashed line) the isotropy breaks down drastically. This is the consequence of the discreteness of space and time. The features of the free-particle regime (2.18) are not so obvious here as in Fig.2.3. Figure (2.10) shows the spectrum of a model with density $\rho = 0.6$. The onset of the lattice regime corresponds to lower values of k, namely $k_1 \simeq 0.25$ as a result of the increase in the mean free path caused by the decrease in density.

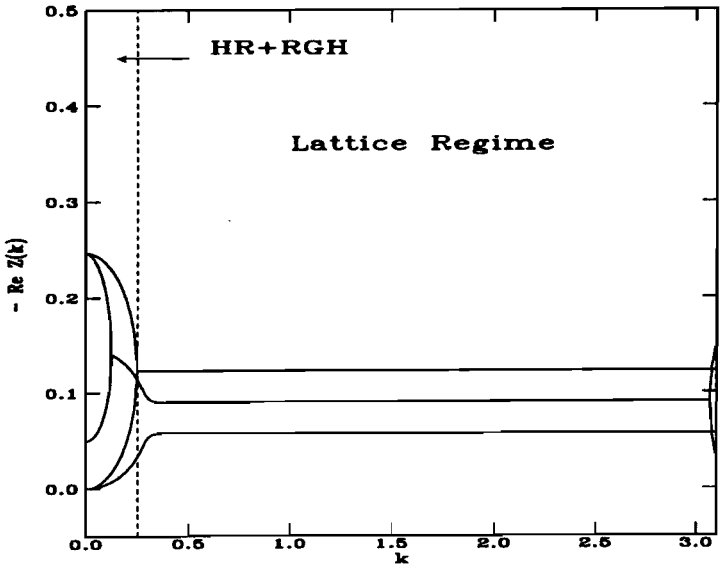

Figure 2.10:
Real part of the spectrum $z_\lambda(\mathbf{k})$, for the six-bit FHP-1 model at $\rho = 0.6$, vs k for $\mathbf{k} \parallel \hat{x}$ axis in reciprocal lattice.

2.4 Spectral analysis of a lattice-gas simulation

Of paramount interest to fluid dynamics is the hydrodynamic regime where the eigenvalue spectrum $z_\lambda(\mathbf{k}) = Rez_\lambda(\mathbf{k}) + iImz_\lambda(\mathbf{k})$ is controlled by long-lived collective excitations. Those spectra define the form of the structure factor $S(\mathbf{k},\omega)$ (1.52), namely at fixed wavelength and scattering angle $\mathbf{k}$ each eigenmode of the spectrum contributes according to (1.64) a spectral line with a maximum located approximately at $Imz_\lambda(\mathbf{k})$ and a width determined by $Rez_\lambda(\mathbf{k})$. The structure factor of a model can be "measured" by running a computer simulation. In such a simulation we examine the spontaneous density fluctuations of a LGCA in equilibrium and compare the simulation results with the theoretical predictions of Sections 1.8 and 1.9 to assess the limits of validity of the Landau-Placzek theory and the Boltzmann evaluation of transport coefficients.

We begin by showing plots of the structure factor as a function of $\mathbf{k}$ at fixed ω, see Fig.2.11. We use the Fast Fourier Transform method of Ref.[28]. The series of 3-dimensional plots present the location of sound peaks in (k_x, k_y) space at four

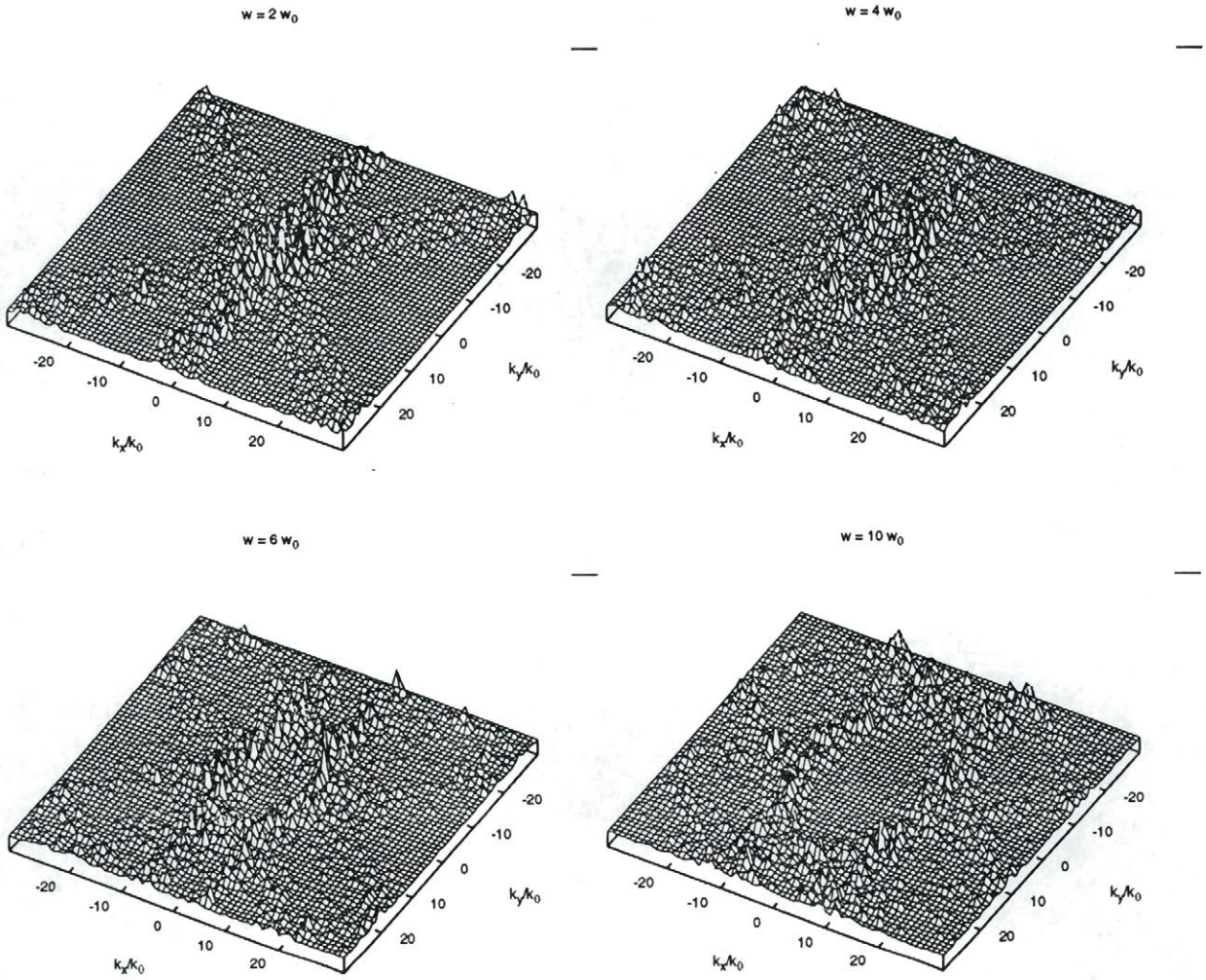

Figure 2.11:
$S(k_x, k_y)$ plots for different ω for the FHP-1 model with density 1.4. The $\hat{y}$ direction of $\mathbf{k}$ vector is scaled with the factor of $\sqrt{3}$ as a result of making the Fourier transform from data defined on triangular lattice.

different frequencies for the FHP-1 lattice gas with density $\rho = 1.4$ and for a lattice of size 64x64. We observe that the peaks form a ring in k-space whose radius increases with increasing ω, in a manner which is supposedly linear for small values of ω. At $\omega = 10\omega_0$ ($\omega_0 = 2\pi/64$ for the total simulation time $t_0 = 64$ time-units) the ring of sound peaks takes a form close to hexagonal. This is because the corresponding $\mathbf{k}$ vectors belong to the lattice regime and hence reflect the symmetry of the underlying lattice. The plots are clearly in qualitative agreement with the Boltzmann analysis.

To perform a more quantitative analysis, it is convenient to work with plots of $S(\mathbf{k},\omega)$ as a function of ω for $\mathbf{k}$ along a particular direction. Figure 2.12 shows the three-dimensional plot of the structure factor (1.52) for the FHP-1 model obtained from the Fourier transformation of the spontaneous density fluctuations. The resulting graph gives the intensity of the spectrum as a function of k_x in reciprocal lattice units $k_0 = 2\pi/128$ and ω in reciprocal time units $\omega_0 = 2\pi/128$. Note that the measured spectrum shows a considerable fluctuation of spectrum amplitude (noise), but gives nevertheless all the important features. The spectrum noise could be "smoothed" by averaging over repeated simulations or over the data for different directions of $\mathbf{k}$ within a single simulation. The latter way would be more efficient in terms of computer time, however, it is valid only for $\mathbf{k}$ vectors inside the hydrodynamic regime, where the LGCA is considered effectively isotropic (See discussion in Sec.2.3).

The simulations were performed with the following specifications: (i) system size of 128x128 and 128 time steps; (ii) periodic boundary conditions; (iii) initialization with zero total momentum i.e. the system is at rest; (iv) measurements were performed after the system has reached equilibrium. (We allowed about 1000 steps, starting from a configuration "guessed" as close to equilibrium as possible). First we note the disagreement of the FHP-1 simulation data with the general form of the structure factor for fluids (1.70): we do not observe the central Rayleigh peak. This is well explained by the fact that the energy in the FHP-1 model is a multiple of the number of particles, hence the transport of energy (caused by gradients of its corresponding

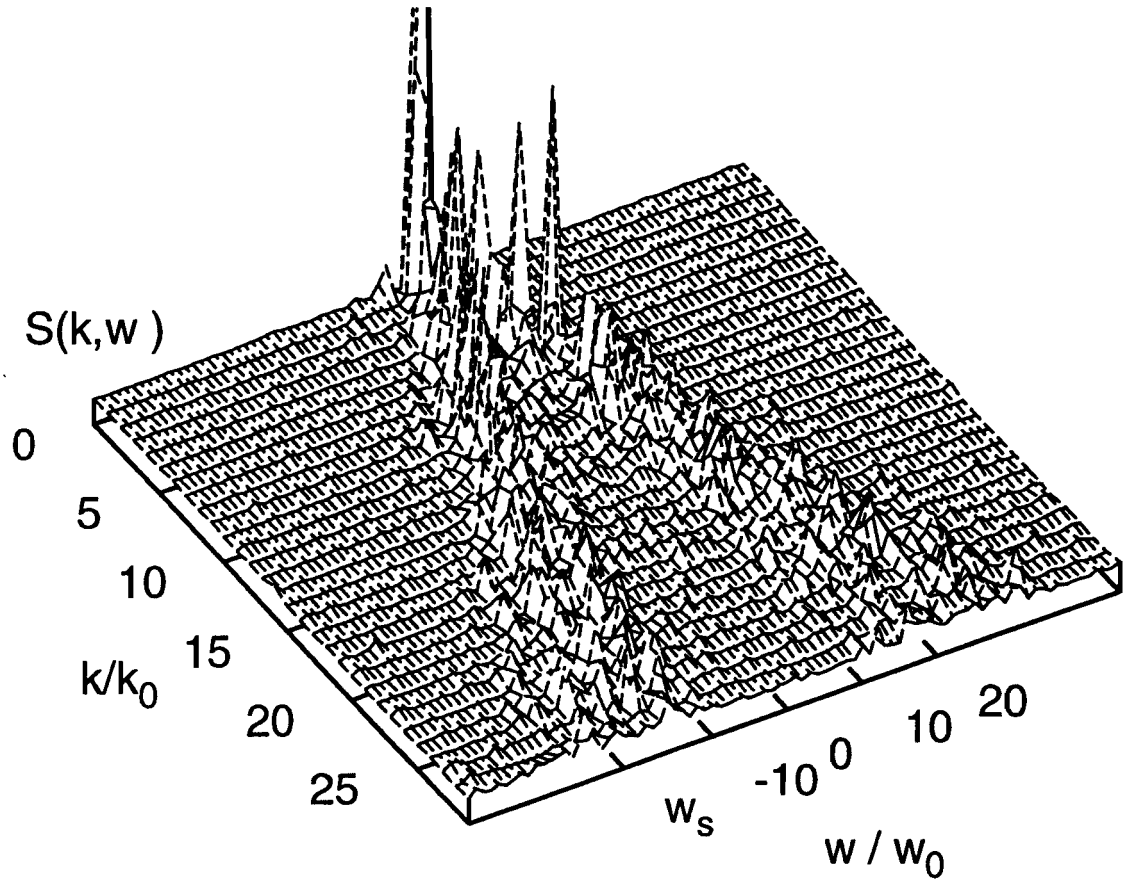

Figure 2.12:
Three dimensional plot of the dynamic structure factor $S(k,\omega)$ as measured from spontaneous fluctuation correlations (lattice size 128x128, number of time-steps 128) for the FHP-1 model with density $\rho = 2.4$. X-Y plane scale: ω is given in reciprocal time-step units $\omega_0 = 2\pi/128$, k is from 0 to 30 in reciprocal lattice units $k_0 = 2\pi/128$ and is directed along $\hat{x}$ axis; vertical scale: intensity of spectrum.

conjugate thermodynamic variable, temperature) is essentially the consequence of the transport of particles.

Further, we study the two symmetrically located Brillouin peaks observed in Fig.2.12 with a width Γk^2 according to (1.70) observed in Fig.2.12. At $k/k_0 = 30$ the location of the sound peak and the linewidth of the sound peak are estimated as $\omega_s/\omega_0 = 22$ and $\Delta\omega_s/\omega_0 = 17$ respectively. From the location of the peaks we can again evaluate the speed of sound, assuming we are in the regime where the relation $\omega_{brillouin} = c_s k$ holds. Note that based on Eq.(1.64), valid for the hydrodynamic regime, and numerical results for the imaginary part of eigenvalue spectrum Figs.2.4 and 2.6, this relation is expected to hold even a little beyond the hydrodynamic regime, in our case up to $k \simeq 0.5$. Thus we evaluate the velocity of sound as $c_s = 0.73$.

Next we use the Landau-Placzek parameterization $\Delta\omega_s(k) = \Gamma k^2$ and analyze the line-widths of Brillouin peaks $\Delta\omega_s$ obtained from the simulation data. At $k = 30k_0 = 30\frac{2\pi}{128}$, $\Delta\omega_s$ has the value $(17 \pm 2)\omega_0$, where $\omega_0 = \frac{2\pi}{128}$. Then the sound damping constant Γ becomes:

$$\Gamma = \frac{\Delta\omega_s}{k^2} = \frac{17\omega_0}{(30k_0)^2} = 0.39 \tag{2.19}$$

All the above results are in good agreement with results for the sound velocity (Fig.2.8) and the sound damping constant (Fig.2.7) calculated from the direct numerical solution of Eq.(1.55). This supports the validity of Eq.(1.55) in the hydrodynamic regime of LGCA and of the FHP-1 model for realistic fluid simulations.

Chapter 3

Thermal Gases

3.1 Introduction

In the FHP-1 model considered in the previous chapter all the particles have the same speed. Therefore the energy of the system is proportional to the number of particles and is not an independent conserved quantity. Hence the grand canonical ensemble (1.21) does not depend on the total system energy, which is equivalent to $\beta = 0$ (an infinite temperature) in (1.21) and all the subsequent formulas. The concept of temperature does not exist for this model. Indeed, the results of computer simulations of the FHP-1 model do not indicate the existence of any temperature related features, such as for example the Rayleigh peak in the structure factor (Fig.2.12). As mentioned in the introduction to Chapter 2 of this thesis, LGCA models of this type are called athermal models.

Obviously the range of applications for athermal models is restricted to the situations where thermal effects do not play an important role. Laminar flow, vortices, turbulence and other phenomena can be simulated by the LGCA athermal models. However in many applications of the LGCA method for realistic fluid dynamics one wishes to use a model which exhibits thermal effects at the macroscopic level. In order to have such systems, with microscopic energy conservation, temperature, temperature gradients, and heat conductivity, we need to have multi-speed models. That

way one can define temperature in accordance with thermodynamics and statistical mechanics.

In this chapter we study the properties of such a thermal model. We approach the problem by asking which multispeed model can be considered as a logical extension of the athermal FHP-1 model studied in Chapter 2. As discussed in Sec.2.1, the inclusion of one additional rest particle does not define the model as a thermal one. Hence the next obvious choice is the so-called 13-bit model, where particles of speed $\sqrt{3}$ or 2 are included, allowing nearest neighbor hops, see Fig. 3.1 for example. However, by inspection, for such a model there are no collisions involving particles of different speeds which conserve both momentum and energy. Although it is possible to construct more general 13-bit models where the energy is not entirely kinetic [12] - or models with particles having different masses [29] which, hence, maximize the number of allowed collisions while conserving mass, momentum, and energy exactly - we will not consider such models in this thesis.

Instead, we will consider models on the triangular lattice, which include six extra allowed velocities with value modulo 2, allowing propagation to next-nearest-neighbors. This 19-bit model does permit collisions which conserve both energy and momentum in a non-trivial manner: we will analyze it in the rest of this chapter.

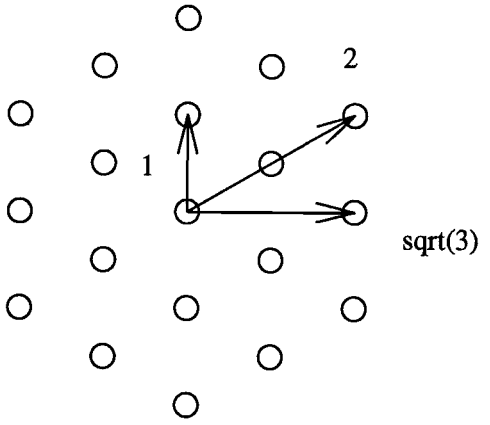

Figure 3.1: Representative velocities for 19-bit model.

3.2 Definition of the 19-bit model

The 19-bit model was introduced by Grosfils *et.al* [21], as a thermal model with non-trivial energy conservation. Particles live on a triangular lattice, where there is one rest particle, and 3 sets of 6 particles with speeds $c = 1, c = \sqrt{3}$, and $c = 2$ and purely kinetic energies $\frac{1}{2}, \frac{3}{2}$ and 2 respectively. Velocities 1 and 2 correspond to displacement by one and two lattice unit lengths, respectively, in one time step along any of the six lattice directions, and velocity $\sqrt{3}$ corresponds to displacement to the next-nearest-neighbor sites along any of the six directions bisecting the lattice directions (see Fig. 3.1). Rest particles reside on the lattice sites. As before, particles obey the exclusion principle (1.23) and undergo collisions according to mass, momentum and energy conservation laws. The 19-bit model is thus a probabilistic LGA with a symmetric transition probability matrix. All transitions between input and output configurations are set to be equally probable for all states which are compatible under the basic conservation laws.

3.3 Constructing the collision table

One of the new features of LGCA of thermal gases as opposed to athermal ones is the considerably larger degree of freedom that is available in the construction of a collision table. In this situation we must pay special attention to the correct choice

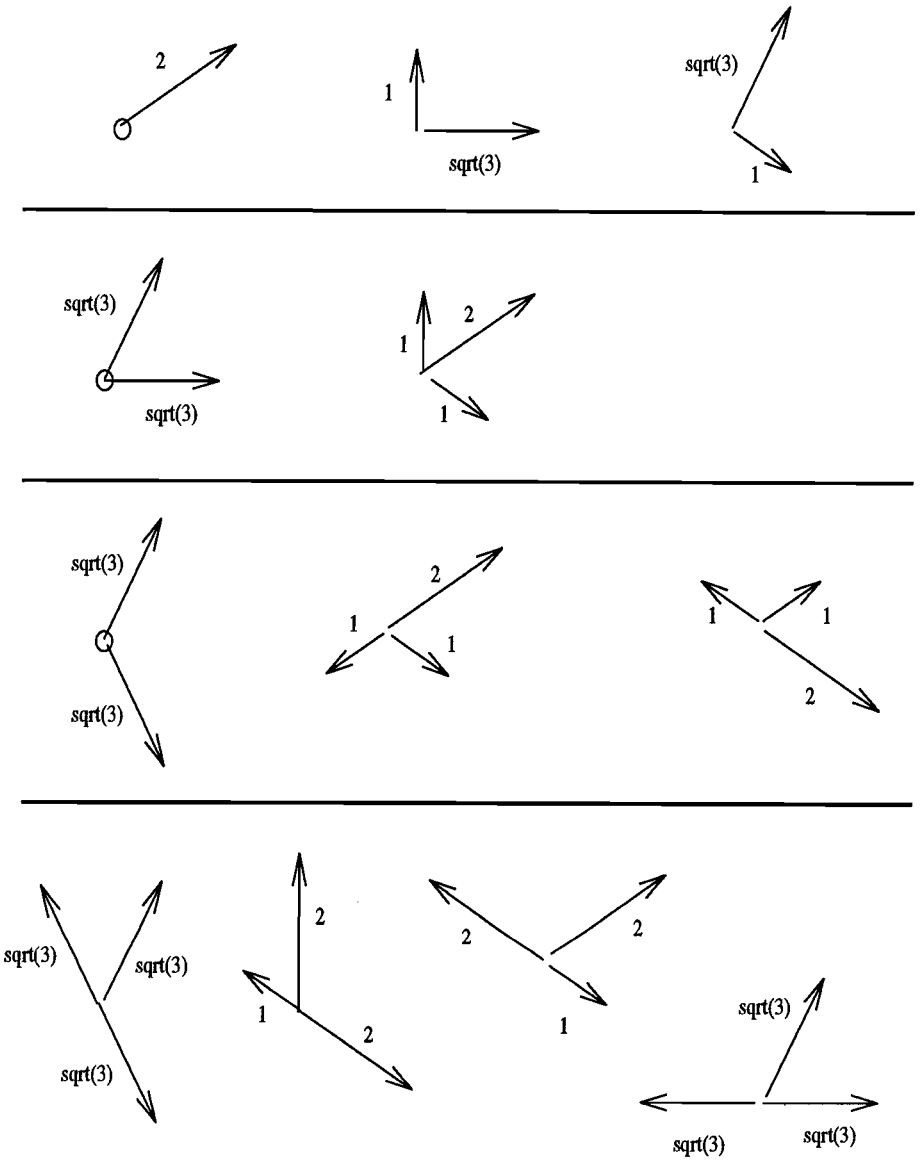

Figure 3.2: elementary configurations for 19-bit model that transfer energy during collision

of collision rules to ensure the proper macroscopic behavior of the lattice gas [1].

The simplest indicator of the suitability of any given collision table is the existence of the universal equilibrium state (see Sec.1.6). We should keep in mind that for thermal models the number of collisions per unit of volume and per unit of time are not the only factors which provide the proper *redistribution of particles* corresponding to the Fermi-Dirac distribution function (1.23). The rapid randomization[2] within one subset of velocities, for example, does not necessarily imply this redistribution. Therefore we are especially interested in collisions that involve particles of different velocities. These are shown in Fig.3.2. We refer to them as the energy transfer collisions and expect them to be responsible for the redistribution of the energy level population to accord with thermal equilibrium.

Since the energy transfer collisions must be included in the collision table, how many of them are enough to provide the proper redistribution? Do we have to include FHP-like collisions rules within some (all) velocity levels? If yes, what is the relation of the number of energy transfer collisions to the total number of collisions? What types of collision table provide the most fluid-like macroscopic behavior of the model? What is the minimum simple set (sets) of collision rules that still ensure good randomization and redistribution of particles among the different velocity channels?

There is no way to answer all the above questions rigorously. Even the analytical expression for the collision frequency in terms of the equilibrium distributions for the 19-bit model involves enormous number of terms as opposed to those for the simple FHP model. Hence we try to answer the above questions by means of "experiments". We run the 19-bit model simulations and "measure" the density fluctuations for models with different collision tables and different parameters. In some cases we also count the number of collisions directly in order to understand the results in terms of the collision frequency and the mean free path.

[1] the original results of Grosfils *et.al* in Refs.[21,30] demonstrate the evident correctness of their choice of collision table, however, they did not clearly specified the collision rules that they used.

[2] randomization of particle configuration was discussed in section (1.6) of this thesis.

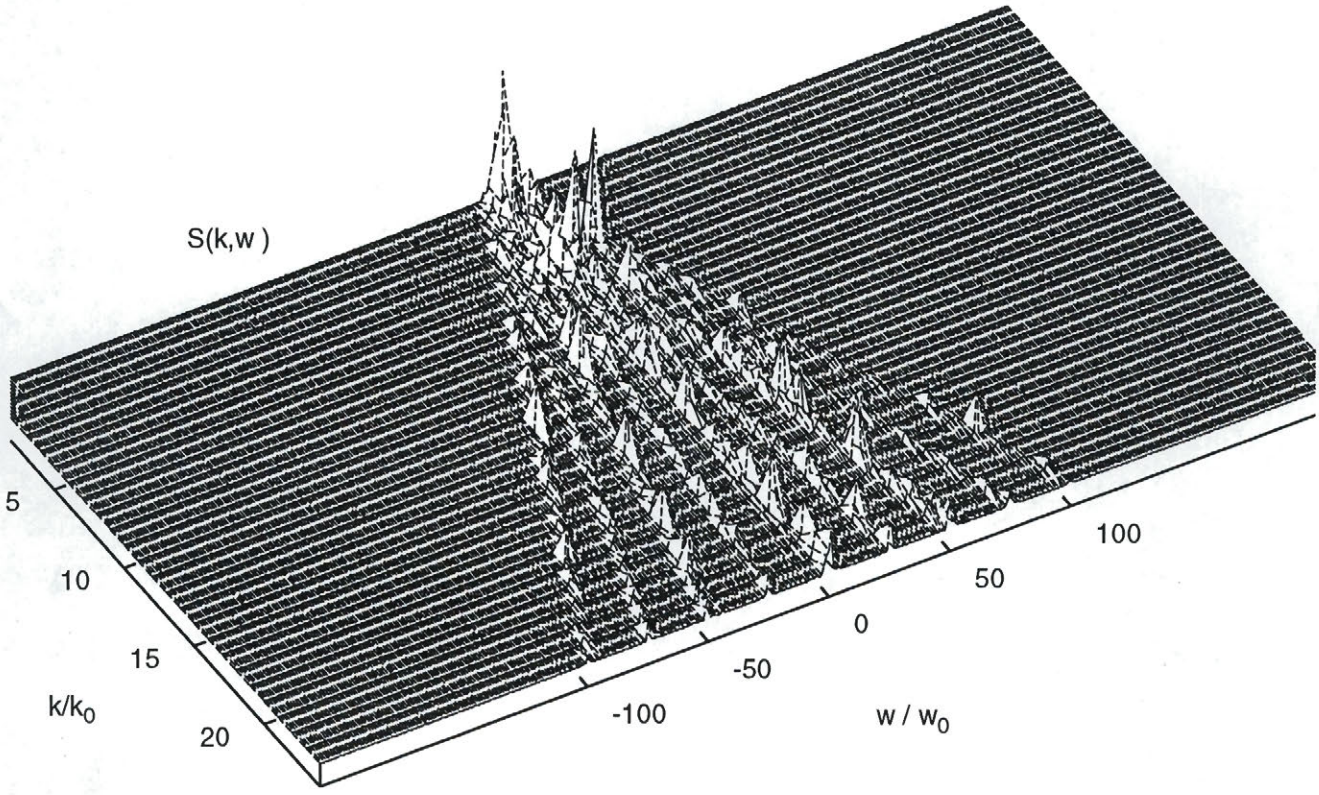

Figure 3.3:
Three dimensional plot of the dynamic structure factor $S(k,\omega)$ as measured from spontaneous fluctuation correlations (lattice size 512x512, number of time-steps 1024) for the 19bit model with density $\rho = 6.0$. The collision table includes the energy transfer collisions (Fig.3.2) only; X-Y plane scale: ω is given in reciprocal time-step units $\omega_0 = 2\pi/1024$, k is from 0 to 25 in reciprocal lattice units $k_0 = 2\pi/512$ and is directed along the $\hat{x}$ axis; vertical scale: intensity of the spectrum. At $k/k_0 = 25$ the five ballistic peaks are located at frequencies 0, 25, 50, 75, 100 respectively in units of ω_0.

First we run the simulation of the 19-bit gas with the collision table shown in Fig.3.2, i.e. with energy transfer collisions only. The three dimensional plot (Fig.3.3) of the dynamic structure factor $S(k,\omega)$ was measured at the density $\rho = 6.0$ and temperature $T = 1/\beta = 5.16$ for wave vectors along the $\hat{x}$ direction and with magnitudes k ranging from 0 to $25 \cdot k_0 = 25 \cdot (2\pi/512) = 0.3$. In the paper of Grosfils et.al. [21] these wave numbers lie inside the hydrodynamic regime which is found to be $k \leq k_h = 0.6$ (discussion of Sec.IV, Fig. 1(a) of the above reference). The total simulation time in our computer experiment is 1024 time-steps. The structure factor (Fig.3.3) does not exhibit the typical line shapes of the Rayleigh-Brillouin spectrum of real fluids. Instead we have 5 ballistic modes corresponding to discrete values of the allowed velocities projected on the $\hat{x}$ axis of the lattice. The result is very much the same as if there were no collisions at all (the so called free particle or ballistic regime). The conclusion is that the density of collisions is too low to provide a mean free path appropriate for the hydrodynamic regime. Indeed, the mean free path for this choice of collision table (energy transfer collisions only) as evaluated from the average number of collisions per one time-step is about 1800 lattice-units (See Table 3.1). This even exceeds the linear lattice size (512).

3.4 Fluid-like behavior of the 19-bit LGCA

There are several possible ways to increase the collision rates so as to produce fluid-like behavior. First we can change the density of the LGCA in order to maximize the probability of the collision configurations of Fig.3.2. We estimate this optimal density approximately as $\rho = 3.0$ since most collisions from Fig.3.2 involve 3 particles at a site. The second way is to expand the collision table by including so called "spectator particles", as defined in Sec.2.1, into the collision rules. Needless to say that this would increase the probability of collisions in the model by several orders of magnitude.

A more effective way is to expand the collision table by including the FHP-like

	Collisions with energy transfer only	Expanded set of collisions (FHP-like included)
collision rate ν_v	$6.8\ 10^{-3}$	$2.3\ 10^{-1}$
mean free path l_0	1800	50

Table 3.1: Collision rates and mean free paths for two different collision tables (simulation result)

collision rules within every subset of velocity channels. Table 3.1 shows the average number of collisions ν_v per site per time-step of evolution for computer simulations of two different 19-bit LGCA: with and without FHP-like collisions. The mean free path l_0 of each case is calculated from Eq.(2.16) where the relevant time scale t_0 is estimated from the number of collisions per unit of time (collision frequency) directly counted during the simulations. Comparing the mean free path l_0 to the linear lattice size (512) we conclude that only in the case of the expanded collision table can we satisfy the condition $kl_0 \ll 1$ for the hydrodynamic regime.

Figure 3.4 shows the result of a simulation with the expanded collision table, but otherwise with exactly the same specifications as in the first case (Fig.3.3). We observe the full Rayleigh-Brillouin spectrum with a well defined central peak, establishing the existence of spontaneous thermal fluctuations.

We see that the spectrum presented in Fig. 3.4 is characteristic of hydrodynamic behavior at long wavelengths. The dynamic structure factor exhibits the typical line shapes of the Rayleigh-Brillouin spectrum in real fluids. It consists of a Brillouin doublet, located at $\omega = \pm c_s k$, where c_s is the sound velocity, and a Rayleigh line centered at $\omega = 0$. In general in the small k domain the spectral density of the lattice-gas fluctuations is consistent with the Landau-Placzek theory. Thus we can make a more quantitatively significant analysis of the spectrum.

We consider the crossection of the structure factor data along the line $k/k_0 = 25$ shown in Fig.3.5. To get better resolution we smoothed the data (See Fig.3.6) using conventional computer routines [31]. The analysis of the Brillouin peaks is similar to

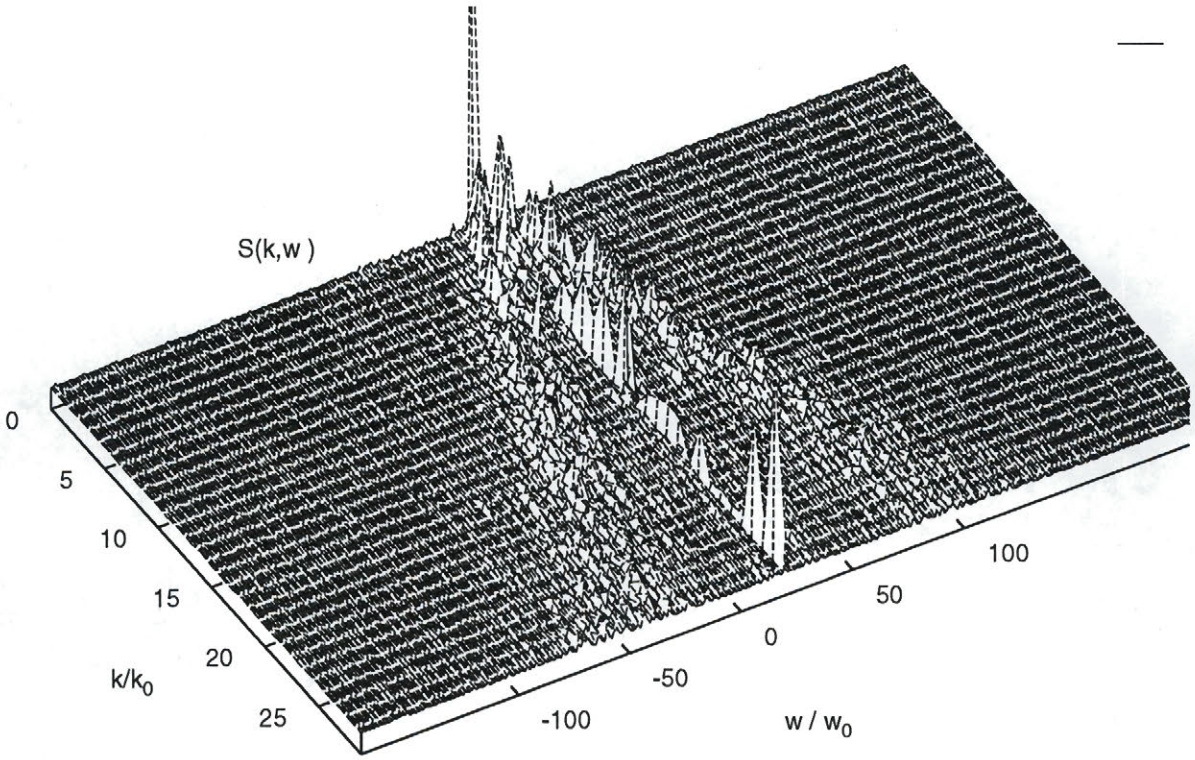

Figure 3.4:
Three dimensional plot of the dynamic structure factor $S(k,\omega)$ as measured from spontaneous fluctuation correlations (lattice size 512x512, number of time-steps 1024) for the 19bit model with density $\rho = 6.0$. The collision table includes the energy transfer collisions (Fig.3.2) only; X-Y plane scale: ω is given in reciprocal time-step units $\omega_0 = 2\pi/1024$, k is from 0 to 25 in reciprocal lattice units $k_0 = 2\pi/512$ and is directed along the $\hat{x}$ axis; vertical scale: intensity of the spectrum. At $k/k_0 = 25$ the sound peaks are located at frequencies +60 and -60 respectively in units of ω_0.

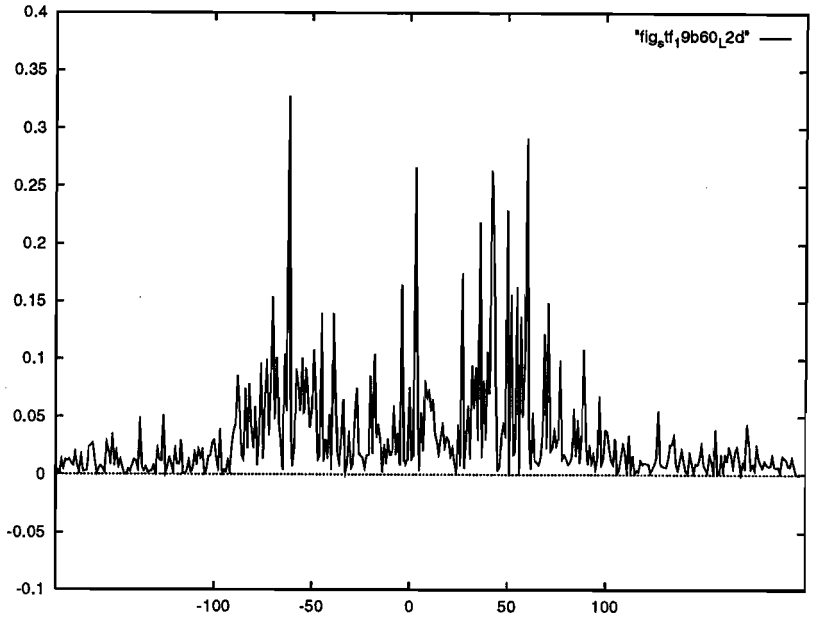

Figure 3.5: Crossection of $S(k,\omega)$ function along $k/k_0 = 25$ line.

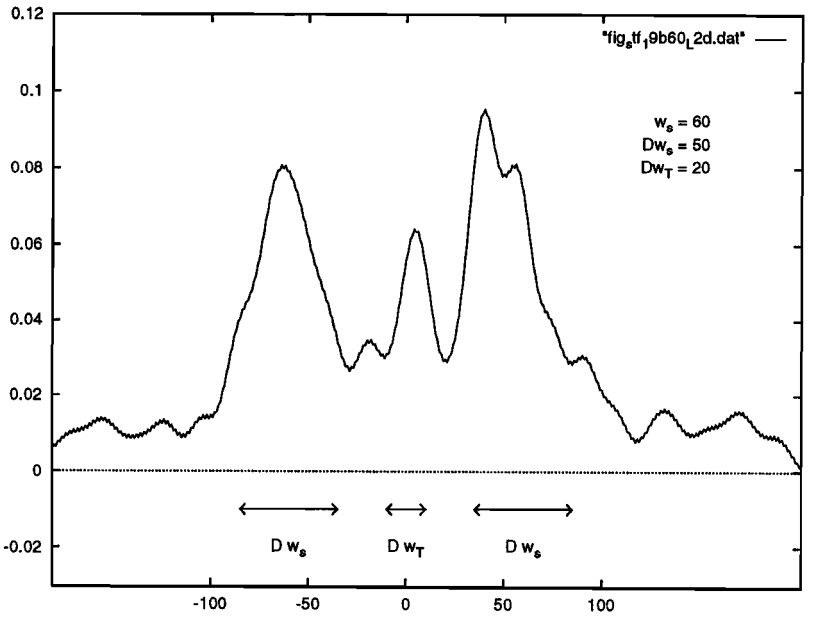

Figure 3.6: Crossection of $S(k,\omega)$ function along $k/k_0 = 25$ line. The result of smoothing procedure [31] of original data, shown in Fig.3.5.

that for the FHP-1 model in Sec. 2.4. For the given value of k the location of the sound peaks is estimated as $\omega_s = \pm 60\omega_0$ (with a tolerance of 5-10%) which gives the value for the sound velocity as $c_s = 1.2 \pm 0.1$. This compares well to the sound velocity $c_s = 1.259$ of the 19-bit model as calculated from the relation (1.31). Furthermore the sound damping constant Γ, evaluated from the width of the sound peaks as shown in Eq.(2.19) is:

$$\Gamma = \frac{50\omega_0}{(25k_0)^2} \simeq 20 \tag{3.1}$$

Similarly, the width of the central Rayleigh peak of Fig.3.6 gives the value for the thermal diffusion coefficient D_T as:

$$D_T = \frac{\Delta\omega_T}{k^2} = \frac{20\omega_0}{(25k_0)^2} \simeq 8 \tag{3.2}$$

These values are very comparable to those obtained from Fig.2(c) of reference [21], suggesting that the mean free path for that model, with density $\rho = 1.1$, was very comparable to that for the present model. Clearly this indicates that we have included fewer collision processes in our simulation than were employed by Grosfils *et.al.* [21].

Chapter 4

Conclusions

In this thesis we have studied the theory of Lattice Gas Cellular Automata, testing the most important aspects of the theory on two lattice gas models on a triangular lattice.

In the first chapter we covered the basic issues of the theory of lattice gases. We concluded that LGCA may be considered as *bona fide*, although extremely simplified, statistical mechanical models, that are able to represent the hydrodynamics and transport properties of fluids. The properties of the equilibrium state and of the transport phenomena were described for the general class of lattice gases with conservation laws for the number of particles, for momentum and for energy. The close parallels with continuous systems were emphasized throughout this chapter. The analysis presented was based on the linear Boltzmann equation, which accounts for short-range spatial correlations (i.e. k dependent transport coefficients), but neglects all memory effects. The present theory, therefore, does not yield any frequency-dependent transport coefficients and is essentially based on a mean field theory.

We considered the simple example of the FHP-1 lattice gas model in Chapter 2. The energy in this model is not an independent conserved quantity, qualifying the model as an athermal one. However, the general theoretical framework of the first chapter is easily adapted to the case of such a model by setting $\beta = 0$ (infinite temperature). Starting from the explicit expressions for the collision matrix of the FHP-1

model we obtained the values of the transport coefficients in Boltzmann approximation, and then numerically studied the properties of the most important quantity in the lattice gas theory - the kinetic propagator (1.53) - by solving the eigenvalue problem (1.55). As a result we obtained the spectra or dispersion relation $z_\lambda(\mathbf{k})$ which provide basic information about the relevant length scales, on the transport coefficients, on the thermodynamic variables, and on the microscopic details of the model.

As a result of our investigations, we consider the following characteristics of LGCA models to be desirable and crucial, so that these models well represent the properties of fluids

- as large as possible a hydrodynamic regime, namely the range of wave-numbers where transport coefficients do not depend on k.
- the isotropy of the fluid dynamical equations, and the absence of spurious invariants.
- sufficient separation of kinetic modes from hydrodynamic ones. According to Eq.(1.48) any averaged quantities not associated with conserved quantities decay exponentially to zero in time. The rate of decay is defined by the kinetic mode values.

For the FHP-1 model with density 2.4 we found the range of the hydrodynamic regime to be $k \leq 0.15$ representing only 5% of the linear size of the Brillouin zone of the reciprocal lattice. Within this regime, the spectra and hence the transport coefficients are independent of the direction of $\mathbf{k}$. We found that with decreasing density the isotropy breaks down at smaller and smaller k values,hence reducing the range of the hydrodynamic regime.

Finally we ran simulations of the FHP-1 model, "experimentally" measuring the dynamic structure factor $S(\mathbf{k},\omega)$. The form of the structure factor also defines the values of the transport coefficients, which were found to be in good agreement with the Boltzmann values.

In Chapter 3 we studied the multi-speed 19-bit model which allows the introduction of local energy conservation into the collision processes. The 19-bit model is a thermal model with well defined thermodynamic temperature and thermal transport properties. The expanded set of allowed velocities increase the number of possible collision tables as compared to FHP-class models. We investigated the results of simulations for two different collision tables and showed the dependence of the macroscopic properties of the LGCA on the value of the mean free path.

We computed the dynamic structure function for the two different collision tables. For one of them we obtained the fluid like form of the structure factor with a well defined central Rayleigh peak, which was not observed in the FHP-1 model. This is a result of the inclusion of the energy conservation into the set of conserved quantities and of the existence of a non-zero subtracted energy current. Again we tested the validity of the model by measuring the wave-number dependence of the frequency of the sound peaks, and of the linewidth of both the central peak and the sound peaks.

The thermal 19-bit model can potentially be applied to a wide variety of interesting physical processes, including phase transitions, as a statistical mechanical model of a fluid. However, the necessity of including the large number of collision rules in the collision table makes the explicit analytical study of the this model almost impossible. For this reason, we feel it would be useful to develop simpler models which nevertheless exhibit the same statistical mechanical properties. We showed (Sec.3.5 and 2.1) that, when the energy is entirely kinetic, non-trivial energy conservation cannot easily be implemented for simpler models such as the 13-bit or the 7-bit models on a triangular lattice even though it is possible for models with potential energy and/or other modified features [29]. However, the possibility of adopting the nontrivial conservation of energy into the lattice gas algorithm and implementing it in this simpler models does exist, we suggest, within the canonical ensemble, where evolution is effectively described by the Monte-Carlo algorithm. This approach seems a promising way to construct LGCA for the modeling of real fluids.

Another reason to search for simpler models arises from attempts to study the

effects of phase transitions on the properties of fluids. The introduction of interactions between particles implies an energy change during the propagation phase of the time evolution. Such a change would require a theoretical analysis going beyond the framework of conventional lattice gas theory and would likely lead to new complications in LGCA theory. In the literature [32] progress has been made by constructing modified models which include effective interactions in the collision phase of the algorithm: unfortunately such models do not obey even semi-detailed balance. Although they display behavior reminiscent of phase transitions - spinodal decomposition and the like - they do not model correct thermodynamics. In our view, further progress requires, again, the study of appropriate thermal LGCA.

References

[1] U. Frisch, B. Hasslacher and Y. Pomeau, Phys. Rev.Lett. **56**, 1 (1986).

[2] D. d'Humières and P. Lallemand, Complex Systems **1**, 599 (1987).

[3] S.P. Das and M.H. Ernst, Physica A **187**, 191 (1992).

[4] J.P. Hansen and I.R. McDonnald, *Theory of Simple Liquids* (Academic Press, London, 1989), p. 10.

[5] N. Goldenfeld, *Lectures on Phase Transitions and the Renormalization Group Theory* (Addison-Wesley Publishing Company, 1993)

[6] U. Frisch, D. d'Humières, B. Hasslacher, P. Lallemand, Y. Pomeau and J.-P. Rivet, Complex Systems **1**, 649 (1987).

[7] Z. Cheng, J.L. Lebowitz and E.R. Speer, Communications on Pure and Applied Mathematics **44**, 971 (1991).

[8] R. Brito and M.H. Ernst, Journal of Physics A **24**, 3331 (1991).

[9] R. Brito, M.H. Ernst and T.R. Kirkpatrick, Journal of Statistical Physics **62**, 283 (1991).

[10] L.P. Kadanoff, G.R. McNamara and G. Zanetti, Phys.Rev A **40**, 4527 (1989).

[11] G. Zanetti, Phys.Rev A **40**, 1539 (1989).

[12] M.H. Ernst and S.P. Das, Journal of Statistical Physics **66**, 465 (1992).

[13] M.H. Ernst, *Microscopic Simulations of Complex Hydrodynamics*, M.Mareschal and B.L.Holian ed. (Plenum, New York, 1992), p. 153.

[14] M.H. Ernst, *Fundamental Problems in Statistical Mechanics VII*, H. van Beijeren ed. (Elsevier Science Publishers B.V., Amsterdam, 1990), p. 321.

[15] R.K. Pathria, *Statistical Mechanics* (Pergamon Press, 1991), p. 142.

[16] S. Chen, M. Lee, K.H. Zhao and G.D. Doolen, Physica D **37**, 42 (1989).

[17] J.J. Binney, N.J. Dowrick, A.J. Fisher and M.E.J. Newman, *The theory of Critical Phenomena* (Oxford University Press, New York, 1992), p. 41.

[18] S. Wolfram, Phys. Rev. Lett. **20**, 1040 (1968).

[19] P. Resibois and M. de Leener, *Classical Kinetic Theory of Fluids* (John Wiley, New York, 1977).

[20] G.E. vanVelzen, S.P. Brito and M.H. Ernst, Journal of Statistical Physics **70**, 811 (1993).

[21] P. Grosfils, J.P Boon, R. Brito and M.H. Ernst, Phys. Rev.E **48**, 2655 (1993).

[22] J.P. Boon and S. Yip, *Molecular Hydrodynamics* (Reprinted by Dover, New York, 1991).

[23] J.A. McLennan, *Introduction to Nonequilibrium Statistical Mechanics* (Prentice Hall, USA, 1989), p. 74.

[24] M.H. Ernst and J.W. Dufty, Journal of Statistical Physics **58**, 57 (1990).

[25] P.J. Davis, *Circulant Matrices* (Wiley, 1979).

[26] S.P. Das, H.J. Bussemaker and M.H. Ernst, Phys. Rev.E **48**, 245 (1993).

[27] J.P. Rivet and U. Frisch, C.R.Acad.Sci.Paris **302**, 267 (1986).

[28] D. Kahaner, C. Moler and S. Nash, *Numerical Methods and Software* (Prentice Hall, 1988).

[29] S. Chen, H. Chen, G.D. Doolen, S. Gutman and M. Lee, Journal of Statistical Physics **62**, 1121 (1991).

[30] P. Grosfils, J.P. Boon and P. Lallemand, Phys. Rev. Lett. **68**, 1077 (1992).

[31] W.H. Press, B.P. Flannery, S.A. Teukolsky and W.T. Vetterling, *Numerical Recipes* (Cambridge University Press, 1986).

[32] D.H. Rothman and S. Zaleski, Reviews of Modern Physics **66**, 1417 (1994).